iScience

CellPress
OPEN ACCESS

Article

TLR2/NF-κB signaling in macrophage/microglia mediated COVID-pain induced by SARS-CoV-2 envelope protein

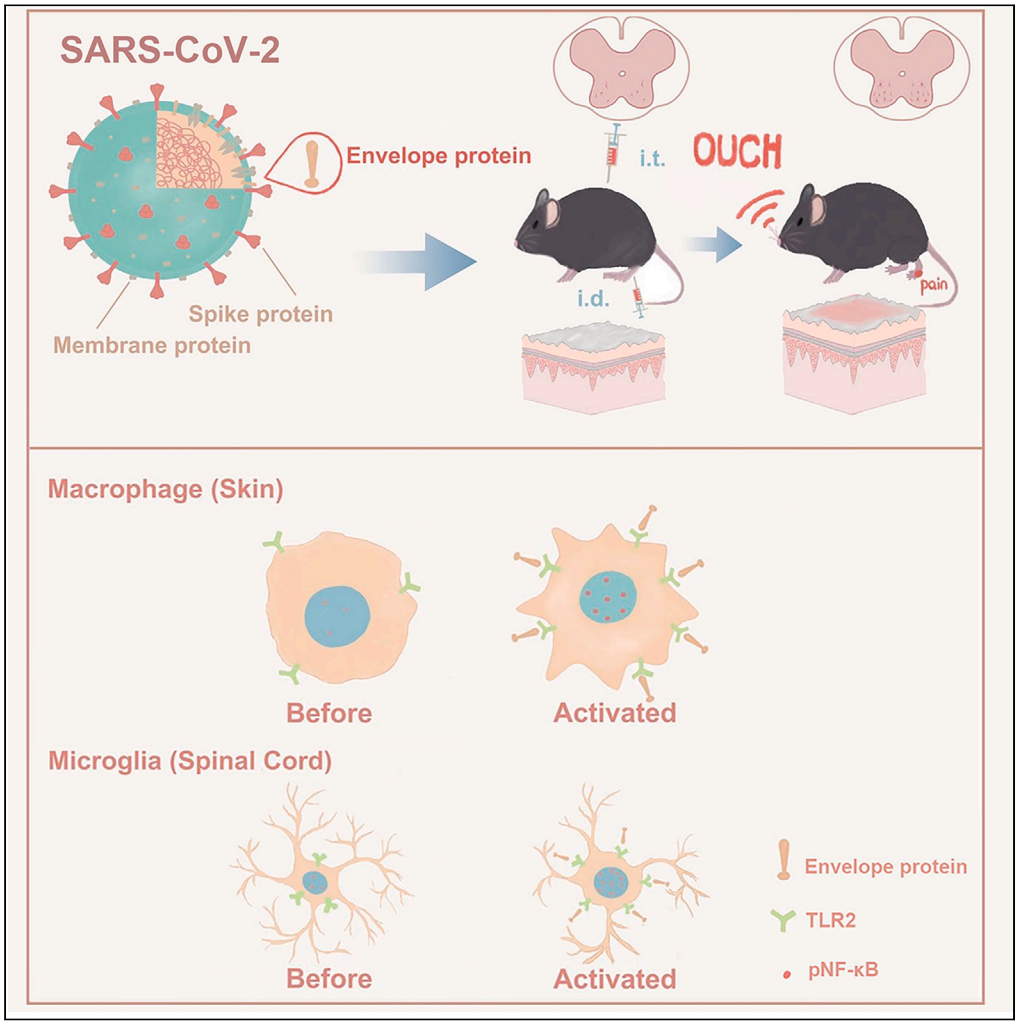

Huan Cui, Fengrun Sun, Ning Yu, ..., Wenying Qiu, Xiangsha Yin, Chao Ma

qiuwy73@126.com (W.Q.)
xiangsha289@126.com (X.Y.)
machao@ibms.cams.cn (C.M.)

Highlights

SARS-CoV-2 membranal proteins are detected in CNS and PNS of COVID-19 donors

SARS-CoV-2 envelope protein, not spike or membrane protein, triggers pain behavior

Targeting macrophage/microglia TLR2 significantly alleviates S2E-induced pain

Cui et al., iScience *27*, 111027
October 18, 2024
https://doi.org/10.1016/j.isci.2024.111027

iScience

CellPress
OPEN ACCESS

Article

TLR2/NF-κB signaling in macrophage/microglia mediated COVID-pain induced by SARS-CoV-2 envelope protein

Huan Cui,[1,5] Fengrun Sun,[1,5] Ning Yu,[1,5] Yan Cao,[1] Xue Wang,[1,2] Di Zhang,[1,2] Zhen Chen,[1,2] Naili Wang,[1,2] Bo Yuan,[1] Penghao Liu,[3] Wanru Duan,[3] Wenying Qiu,[1,2,*] Xiangsha Yin,[1,2,*] and Chao Ma[1,2,4,6,*]

SUMMARY

Pain has become a major symptom of long COVID-19 without effective therapy. Apart from viral infection pathological process, SARS-CoV-2 membranal proteins (envelope [S2E], spike [S2S] and membrane [S2M]) also present pro-inflammatory feature independently. Here, we aim to uncover the neuroinflammatory mechanism of COVID-pain induced by SARS-CoV-2 membranal proteins. We detected the three proteins in both peripheral sensory ganglions and spinal dorsal horn of COVID-19 donors. After intradermal and intrathecal injection, only S2E triggered pain behaviors, accompanied with upregulated-phosphorylation nuclear factor kappa B (NF-κB), which was significantly attenuated by minocycline in mice. We further identified Toll-like receptor 2 (TLR2) among TLRs as the target of S2E to evoke inflammatory responses leading to COVID-pain. This study identified the nociceptive effect of S2E through directly interacting with macrophage/microglia TLR2 and inducing the following NF-κB inflammatory storm. Clearing away S2E and inhibiting macrophage/microglia TLR2 served as perspective therapeutic strategies for COVID-19 pain.

INTRODUCTION

The global coronavirus disease 2019 (COVID-19) pandemic, stemming from severe acute respiratory syndrome coronavirus 2 (SARS-CoV-2) infection, initially manifests with classical symptoms including fever, cough, and fatigue.[1] However, recent studies have unveiled an additional layer of complexity, wherein SARS-CoV-2 induces a spectrum of neurological symptoms, encompassing pain, hyposmia, stroke, and depression.[2–10] Among the manifold symptoms experienced by COVID-19 patients, pain symptoms are frequently reported, including sore throat, myalgia/arthralgia, chest pain, abdominal pain, and headache.[11] Of particular significance is the observation that COVID-19-related pain persists long after the resolution of respiratory symptoms, emerging as a predominant concern in long COVID-19.[5,12–14] Furthermore, it has been reported that primary pain can be aggravated during SARS-CoV-2 infection.[15] Moreover, increasing evidence has revealed a higher frequency and intensity of pain manifestation in female COVID-19 patients, suggesting the potential sex disparities in the involvement of the sensory system.[16,17]

Regarding the pain symptoms observed in COVID-19, it is imperative to consider the dysfunction of elements within the sensory system, potentially triggered by direct viral infection and/or secondary neuroinflammatory processes. Evidences have pointed that dysregulating immune cells such as exhausted T cells and reduced $CD4^+$ and $CD8^+$ effector memory cell numbers, could extremely persist for more than 13 months, along with elevated levels of cytokines including IL-1β, IL-6, and TNFα.[18] Indeed, SARS-CoV-2 has been detected in human cerebrospinal fluid, concomitant with associated neuroinflammation and tissue damage in COVID-19 patients.[19–21] It has been reported that the classical markers related to sensory nervous system such as substance P (SP) and transient receptor potential vanilloid1 (TRPV1) were significantly upregulated after SARS-CoV-2 infection and might be linked to acute and chronic cough.[22] Nevertheless, the detailed mechanism of pain symptoms in COVID-19 patients is still unclear.

SARS-CoV-2 is an enveloped, single-stranded RNA β-coronavirus, assembled by four major proteins: the spike (S), nucleocapsid (N), membrane (M), and envelope (E) protein.[23,24] While the SARS-CoV-2 S protein (S2S) is primarily responsible for host cell recognition via

[1]State Key Laboratory of Common Mechanism Research for Major Diseases, Department of Human Anatomy, Histology and Embryology, Neuroscience Center, Joint Laboratory of Anesthesia and Pain, Institute of Basic Medical Sciences Chinese Academy of Medical Sciences, School of Basic Medicine Peking Union Medical College, No.5 DongDanSanTiao, Dongcheng District, Beijing 100005, China
[2]National Human Brain Bank for Development and Function, Beijing, China
[3]Department of Neurosurgery, Xuanwu Hospital, Capital Medical University, Laboratory of Spinal Cord Injury and Functional Reconstruction, China International Neuroscience Institute (CHINA-INI), Beijing, China
[4]Chinese Institute for Brain Research, Beijing 102206, China
[5]These authors contributed equally
[6]Lead contact
*Correspondence: qiuwy73@126.com (W.Q.), xiangsha289@126.com (X.Y.), machao@ibms.cams.cn (C.M.)
https://doi.org/10.1016/j.isci.2024.111027

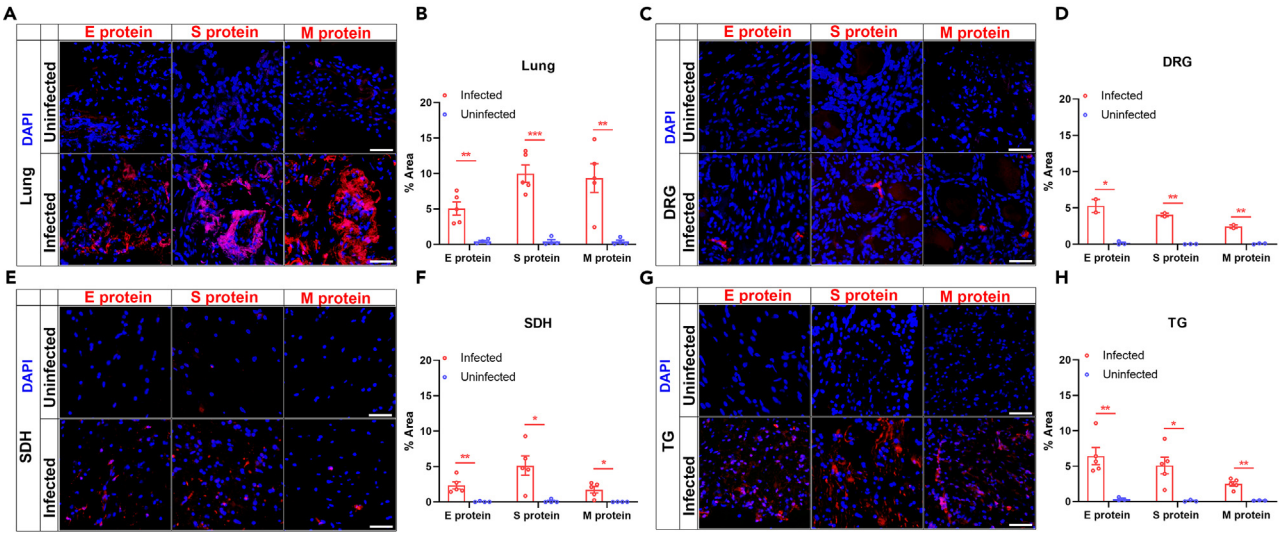

Figure 1. Identification of several coat proteins of SARS-COV-2 in human tissues

(A, C, E, and G) Immunostaining detected the presence of S2E, S2S, and S2M (red) in the lung, SDH, DRG, and TG from COVID-19 infected donors, but not in the uninfected tissues (blue for DAPI). Scale bar: 50 μm.

(B, D, F, and H) Quantitative analysis of S2E, S2S, and S2M positive area percentages in lung, SDH, DRG and TG from infected donors. $*p < 0.05$, $**p < 0.01$, $***p < 0.001$, Student's t test.

angiotensin-converting enzyme 2 (ACE2), the function and pathological characteristics of the SARS-CoV-2 N protein (S2N), SARS-CoV-2 M protein (S2M), and SARS-CoV-2 E protein (S2E) require further elucidation. S2E, the smallest integral membranal protein, typically participates in viral assembly, budding and intracellular transport. It has been detected in lung tissues, microvascular endothelial cells, and cerebrospinal fluid.[25–28] Additionally, S2E functions as a virulence factor via its ion channel activity and provokes a robust immune response, the absence of which significantly diminishes SARS-CoV-2 pathogenicity and attenuates inflammatory signaling.[29] Furthermore, S2E can independently induce pathological damage resembling acute respiratory distress syndrome by activating Toll-like receptor 2 (TLR2) on macrophages and triggering the secretion of cytokines and chemokines.[30] However, whether E protein can directly induce neuroinflammation and its contribution to SARS-CoV-2 related pain remain unclear. In this study, we have investigated the pain-like behaviors in both male and female mice following the intradermal injection or intrathecal injection of three viral membrane proteins of SARS-CoV-2 and explored potential inflammation-associating mechanism, which would supply probable therapeutic strategy for viral infection associated pain symptoms.

RESULTS

Detection of SARS-CoV-2 membranal proteins in PNS and CNS of COVID-19 patients

Given that the virus coat membrane is the initial critical element in infecting the organs and cells, we first ascertained the presence of membranal proteins S2E, S2S, and S2M in human donors' lungs and nervous system including the spinal cord dorsal horn (SDH), dorsal root ganglion (DRG), and trigeminal ganglion (TG). We distinguished the infected/uninfected patient by whether the positive fluorescence signal could be detected in the lung. As expected, all three membranal proteins were found in infected patients' lungs (Figure 1A). Subsequently, we estimated the extent of expression of these membrane proteins within different tissues by the percentage of positive signal area (Figure 1B). Inspiringly, we also found S2E, S2S, and S2M in SDH, DRG, as well as TG of infected patients (Figures 1C–1H), whereas the positive signals of these three membranal proteins were not found in infectors' tissues using the isotype control IgG antibody (Figure S1). In summary, the membranal protein of SARS-CoV-2 could infect both the respiratory system, peripheral nervous system (PNS), and central nervous system (CNS), indicating the possibility of SARS-CoV-2 membranal protein to evoke pain.

S2E, but not S2S or S2M, induced pain

Considering that among the three membranal proteins, S2E appeared to have the potential to induce a series of neuropathologic effects such as depression-like behaviors, dysosmia and neuroinflammation in CNS through interacting with TLR2,[31] we first applied S2E intradermal (i.d.) injection to observe its peripheral nociceptive impact in male and female mice. The results indicated that S2E evoked mechanical allodynia to 0.4 g von Frey stimuli and thermal hyperalgesia compared to phosphate-buffered saline (PBS). Notably, S2E produced a dose-dependent nociceptive effect in PNS (Figures 2A–2D). In contrast, the remaining membranal proteins, including S2S and S2M, failed to induce allodynia to von Frey filaments or hyperalgesia to thermal stimulus following injection (Figures 2E–2H, S2A, and S2B). Notably, the S2E-induced hypersensitivity effects gradually faded away and could only sustain for less than 24 h. Besides, no obvious sex difference was observed in S2E-induced pain-like behaviors.

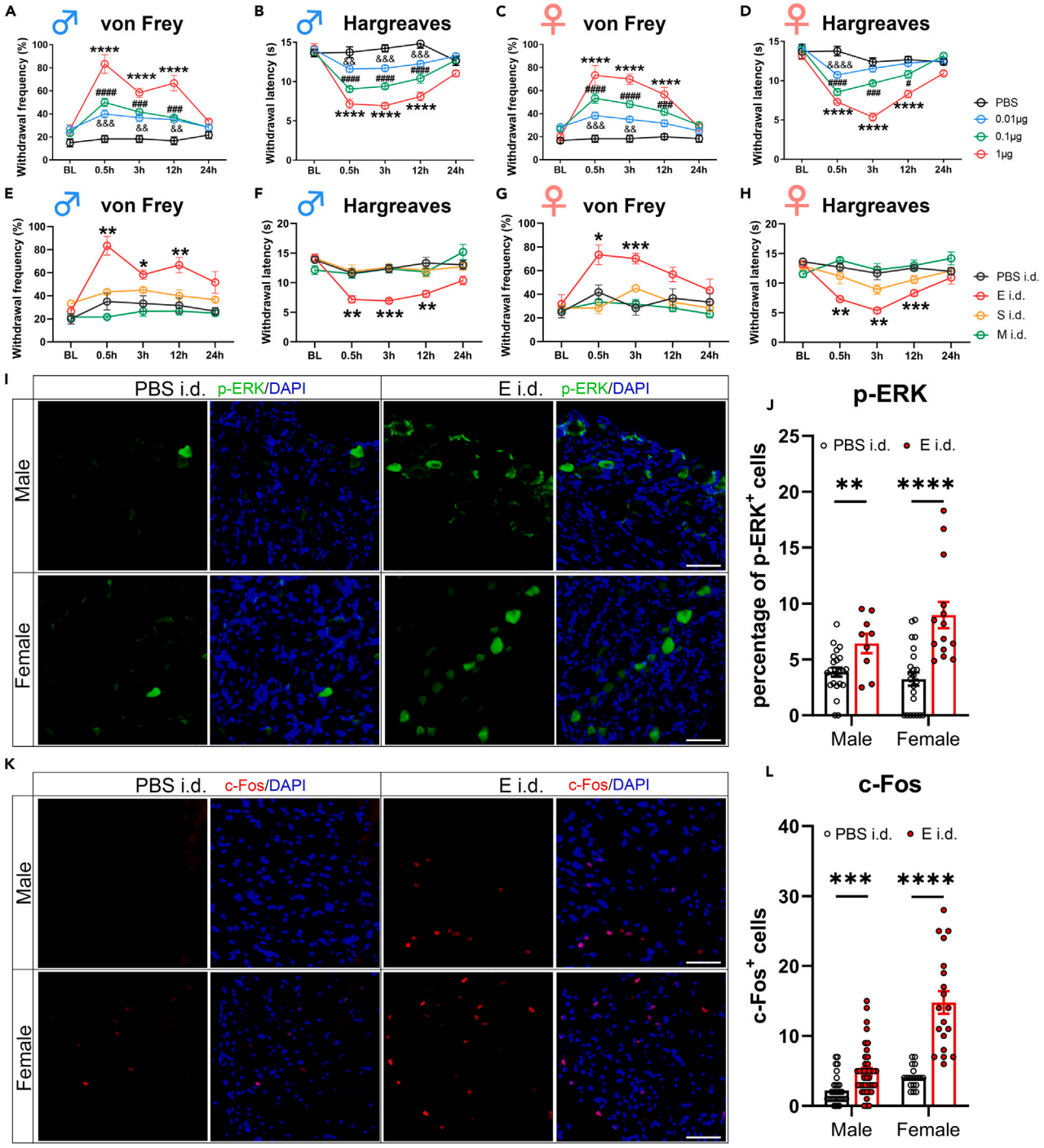

Figure 2. The algesiogenic effects of SARS-CoV-2 viral proteins via i.d. injection

(A–D) Paw withdrawal frequency to 0.4 g von Frey filament and withdrawal latency in Hargreaves test of male and female mice after i.d. injection of S2E with gradually increasing doses (0.01 μg, 0.1 μg, and 1 μg). $n = 6$ mice/group. $^{\#}p < 0.05$, $^{\&\&}p < 0.01$, $^{\&\&\&}$ or $^{\#\#\#}p < 0.001$, **** or $^{\#\#\#\#}$ or $^{\&\&\&\&}p < 0.0001$ vs. PBS, two-way ANOVA for repeated measures followed by Dunnett's multiple comparisons test. (BL: Baseline).

(E–H) Paw withdrawal frequency to 0.4 g von Frey filament and latency in male and female mice after i.d. application of PBS, S2E, S2S, and S2M (1 μg). $n = 6$ mice/group; $^{*}p < 0.05$, $^{**}p < 0.01$, $^{***}p < 0.001$ vs. PBS, two-way ANOVA for repeated measures followed by Dunnett's post hoc test. (BL: Baseline).

(I and J) Immunofluorescence of *p*-ERK (green) in DRG from mice receiving i.d. injection of PBS or S2E, along with quantitative analysis (blue for DAPI). Scale bar: 50 μm $n = 3$ mice/group. $^{**}p < 0.01$, $^{****}p < 0.0001$, Student's t test.

(K and L) Immunofluorescence of c-Fos (red) in SDH from mice receiving i.d. injection of PBS or S2E (blue for DAPI), along with quantitative analysis. Scale bar: 50 μm $n = 3$ mice/group. $^{***}p < 0.001$, $^{****}p < 0.0001$, Student's t test.

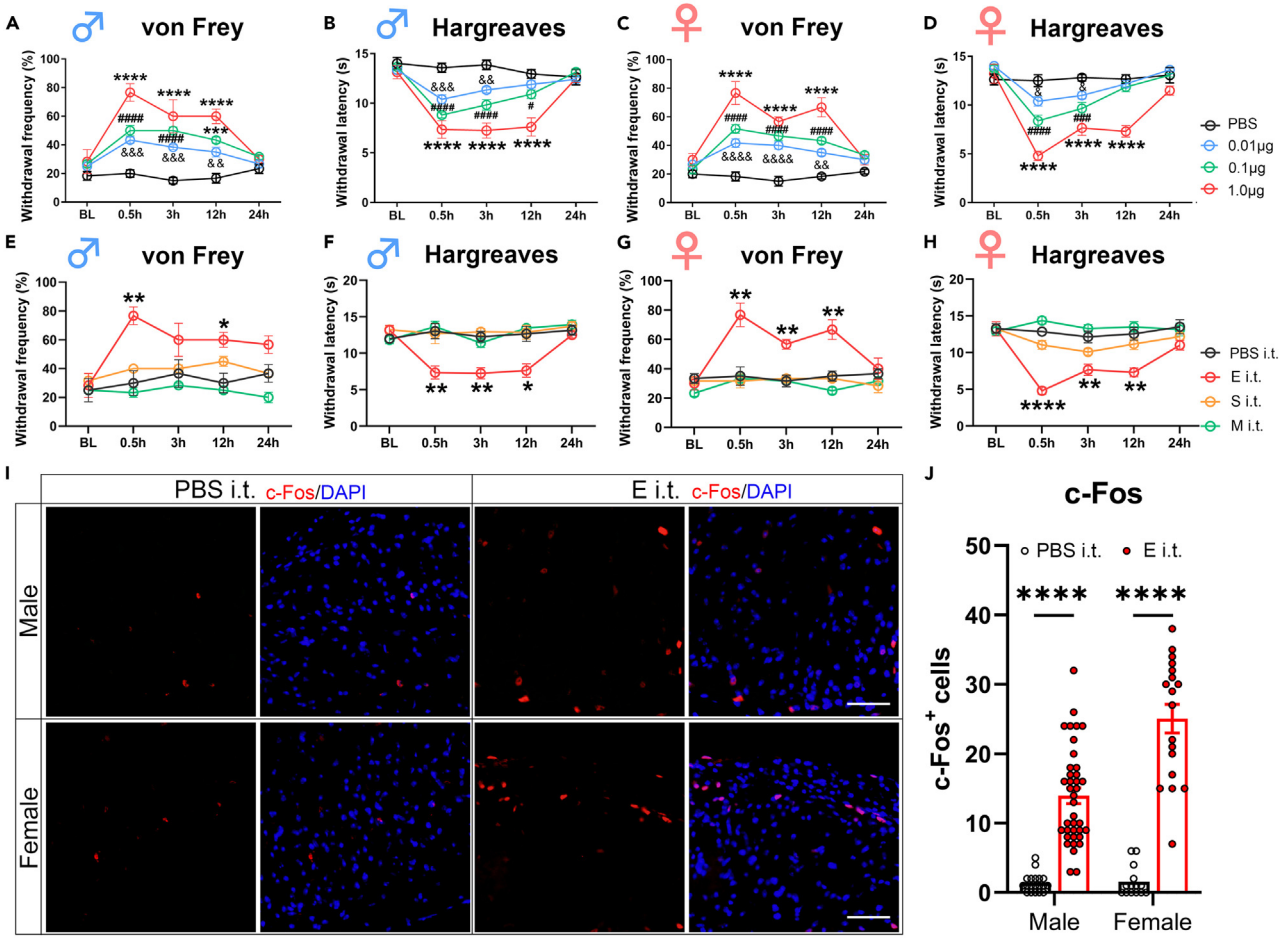

Figure 3. The algesiogenic effects of SARS-CoV-2 viral proteins via i.t. injection

(A–D) Paw withdrawal frequency to 0.4 g von Frey filament and withdrawal latency in Hargreaves test of male and female mice after i.t. injection of S2E with gradually increasing doses (0.01 μg, 0.1 μg and 1 μg). $n = 6$ mice/group. $^{\#}$ or $^{\&}p < 0.05$, $^{\&\&}p < 0.01$, *** or $^{\#\#\#}$ or $^{\&\&\&}p < 0.001$, **** or $^{\#\#\#\#}$ or $^{\&\&\&\&}p < 0.0001$ vs. PBS, two-way ANOVA for repeated measures followed by Dunnett's multiple comparisons test. (BL: Baseline).

(E–H) Paw withdrawal frequency and latency in male and female mice after i.t. application of PBS, S2E, S2S, and S2M (1 μg). $n = 6$ mice/group; $^{*}p < 0.05$, $^{**}p < 0.01$, $^{****}p < 0.0001$ vs. PBS, two-way ANOVA for repeated measures followed by Dunnett's post hoc test. (BL: Baseline).

(I and J) Immunofluorescence of c-Fos (red) in SDH from mice receiving i.t. injection of PBS or S2E (blue for DAPI), along with quantitative analysis. Scale bar: 50 μm $n = 3$ mice/group. $^{****}p < 0.0001$, Student's t test.

To delve into the underlying mechanisms, we examined the activation of neuronal pathways using *p*-ERK and c-Fos as markers after noxious stimulation or tissue injury. Immunostaining revealed that both *p*-ERK expression in DRG and c-Fos expression in SDH were significantly increased after intradermal injection of S2E in male and female mice (Figures 2I–2L). Subsequently, we employed intrathecal (i.t.) injection of SARS-CoV-2 membranal proteins to simulate virus invasion to CNS. Behavioral assay suggested that both male and female mice exhibited a marked increase in paw withdrawal frequency in response to 0.4 g von Frey filament and decreased withdrawal latency to heat stimulation in a dose-dependent manner following S2E i.t. application at incremental doses (Figures 3A–3D). In contrast, i.t. injection of S2S and S2M did not induce pain-like behaviors compared to vehicle PBS (Figures 3E–3H, S2C, and S2D). As expected, the expression of c-Fos in SDH and *p*-ERK in DRG were also induced by i.t. application of S2E, whereas the percentage of *p*-ERK^{+} neurons (Male: 4.24%, Female: 5.06%) was much lower than i.d. model (Male: 6.43%, Female: 8.98%) (Figures 3I–3J and S3). Importantly, we did not detect itch-like behavior as both i.d. and i.t. injection of S2E in male and female mice, implying that S2E elicited a pain-specific response (Figures S4A and S4B). These previous data suggested that S2E invasion of PNS and CNS could induce pain.

Since the commercial S2E was purified from *E.coli*, it was noteworthy whether the allodynia was induced by lipopolysaccharide (LPS), which was identified to activate TLR4 and the downstream signaling pathway.[32] We estimated the LPS content by limulus amebocyte lysate (LAL) assay in 1 μg of the commercial S2E protein solution to be 0.15 EU, of which the content was much less than the minimal dose for LPS (1 μg per mice) to evoke allodynia.[33,34] To further exclude the potential effects of LPS, we performed neutralization by pre-incubating S2E and polymyxin B (PMB), an antimicrobial peptide with LPS-binding affinity to aggregate in large micelles.[32] The co-administration of PMB and S2E

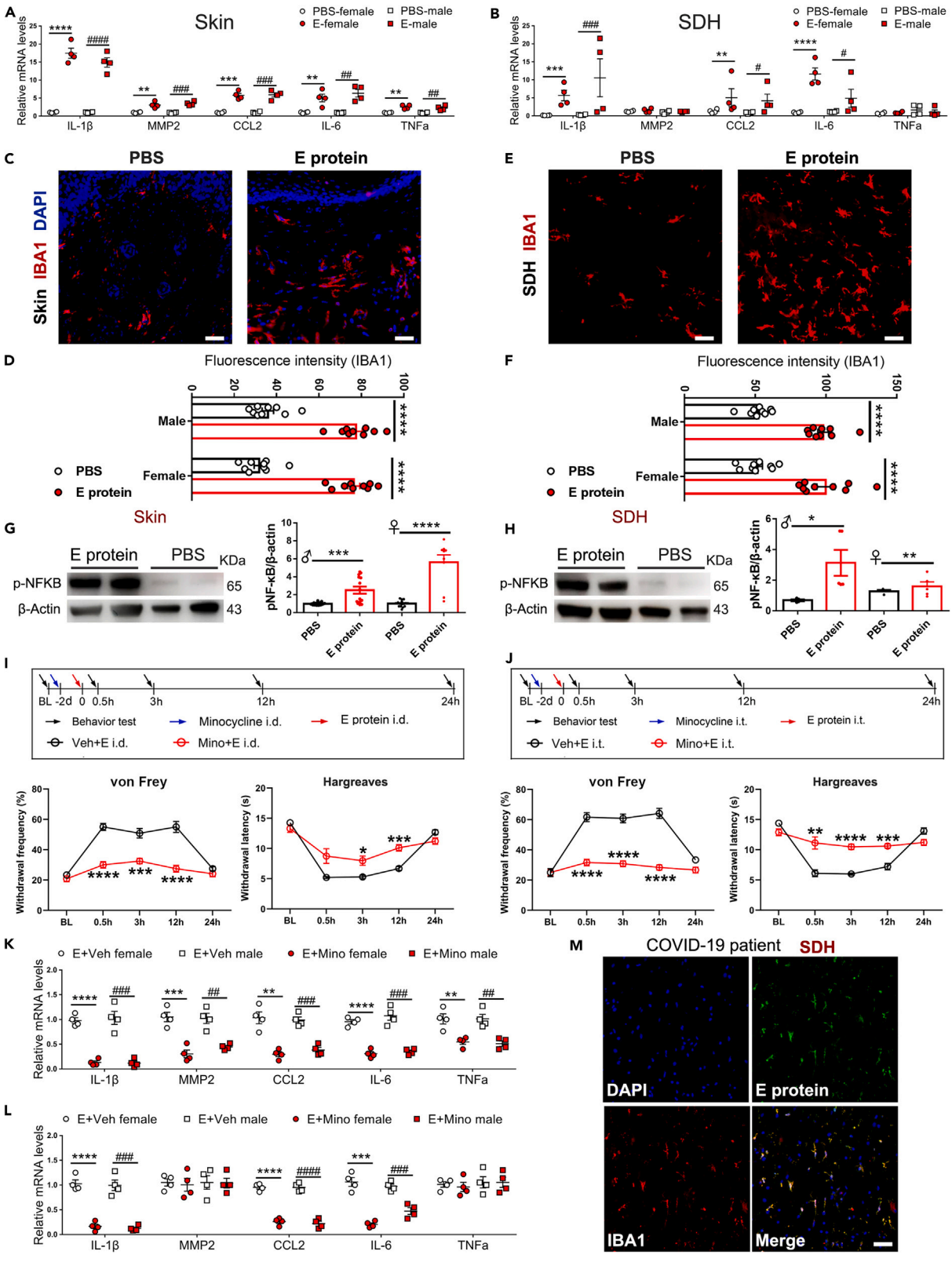
A
Skin
PBS-female
PBS-male
E-female
E-male
Relative mRNA levels
IL-1β
MMP2
CCL2
IL-6
TNFa
B
SDH
C
PBS
E protein
Skin
IBA1
DAPI
D
Fluorescence intensity (IBA1)
Male
Female
PBS
E protein
E
SDH
F
G
Skin
p-NFKB
β-Actin
KDa
65
43
pNF-κB/β-actin
H
SDH
I
BL -2d 0 0.5h 3h 12h 24h
Behavior test
Minocycline i.d.
E protein i.d.
Veh+E i.d.
Mino+E i.d.
J
Minocycline i.t.
E protein i.t.
Veh+E i.t.
Mino+E i.t.
von Frey
Withdrawal frequency (%)
Hargreaves
Withdrawal latency (s)
K
E+Veh female
E+Veh male
E+Mino female
E+Mino male
L
M
COVID-19 patient
SDH
DAPI
E protein
IBA1
Merge

Figure 4. Deletion of macrophage/microglia alleviated S2E-induced pain and inflammation

(A and B) q PCR analyzed the mRNA levels of IL-1β, MMP2, CCL2, IL-6, and TNFα in the skin and SDH after PBS or S2E treatment. $^{\#}p < 0.05$, **or $^{\#\#}p < 0.01$, *** or $^{\#\#\#}p < 0.001$, **** or $^{\#\#\#\#}p < 0.0001$, Student's t test.

(C–F) Immunofluorescence of IBA1 (red) in skin (C and D) and SDH (E and F) (blue for DAPI), along with quantification of IBA1 fluorescence intensity. Scale bar: 50 μm $n = 3$ mice/group. $^{****}p < 0.0001$, Student's t test.

(G and H) Western blotting analysis of p-NF-κB in skin and SDH from PBS or S2E treated mice. $^{*}p < 0.05$, $^{**}p < 0.01$, $^{***}p < 0.001$, $^{****}p < 0.0001$, Student's t test.

(I and J) Behavioral tests revealed that mechanical allodynia (0.4 g von Frey filament) and thermal hyperalgesia induced by S2E were inhibited by minocycline. $n = 6$ mice/group in both sexes. $^{*}p < 0.05$, $^{**}p < 0.01$, $^{***}p < 0.001$, $^{****}p < 0.0001$, two-way ANOVA for repeated measures followed by Sidak's post hoc test. (BL: Baseline).

(K and L) qPCR analyzed the mRNA expressions of IL-1β, MMP2, CCL2, IL-6 and TNFα in the skin (K) and SDH (L) from S2E-treated mice with the application of minocycline or vehicle. ** or $^{\#\#}p < 0.01$, *** or $^{\#\#\#}p < 0.001$, **** or $^{\#\#\#\#}p < 0.0001$, Student's t test.

(M) Co-labeling of E protein (green) and IBA1 (red) in SDH from a COVID-19 infected patient (blue for DAPI). Scale bar: 50 μm.

made no sense on the pain behavior compared to administrating S2E alone, and it indicated the mechanical allodynia and heat hyperalgesia were actually evoked by S2E (Figure S5).

Macrophage/microglia mediated S2E-related pain

We speculated that S2E, acting as an external invasive substance, might elicit pain through the induction of neuroinflammation. Therefore, we first tested pain-related cytokines in the skin (for i.d. model) and SDH (for i.t. model). qPCR results showed upregulation of IL-1β, MMP2, CCL2, IL-6, and TNFα in the skin and upregulation of IL-1β, CCL2, and IL-6 in the SDH (Figures 4A and 4B). It has been regarded that peripheral macrophages and central microglia belong to the same lineage, which were essential in the process of pathogen defense and innate immune regulation.[35] Therefore, we performed immunofluorescence test to investigate the effects of S2E on macrophage and microglia reactivity. The results showed that i.d. injection of S2E increased IBA1 expression in the skin while i.t. injection of S2E upregulated IBA1 in the SDH, indicating that macrophage/microglia may be involved in S2E-induced pain through their activation (Figures 4C–4F). Furthermore, we examined the phosphorylation of nuclear factor kappa B (NF-κB), a classic downstream signal of the TLRs pathway, which became activated when TLRs encounter external pathogens. Western blotting results showed that S2E, compared to vehicle PBS, significantly upregulated p-NF-κB in skin (for i.d. model) and SDH (for i.t. model) (Figures 4G and 4H). However, the level of the unphosphorylated form of NF-κB remained unchanged after S2E stimulation, suggesting the activation of TLR2-NF-κB signaling induced by S2E (Figures S6A and S6B).

To investigate the role of skin macrophage and SDH microglia in S2E-related pain, we utilized minocycline to inhibit macrophage/microglia via suppressing pro-inflammatory polarization,[36,37] and observed its impact on pain behavior. For i.d. model, behavioral assay indicated that pre-application of minocycline could significantly alleviate mechanical allodynia and thermal pain induced by S2E in both male and female mice (Figures 4I and S7A). Similarly, in the S2E i.t. injection model, pre-application of minocycline also markedly attenuated mechanical allodynia, as well as thermal hyperalgesia, compared to vehicle (Figures 4J and S7B). We then evaluated the protein level of p-NF-κB in the skin and SDH from mice receiving minocycline treatment using western blotting. The results revealed that application of minocycline significantly reduced the expression of p-NF-κB in the skin and SDH of S2E-treated mice without significant change of NF-κB expression (Figures S6C, S6D, and S8). Consistent with the previous findings, the mRNA levels of IL-1β, MMP2, CCL2, IL-6, and TNFα in the skin were downregulated in the minocycline-treated mice, while only the expressions of IL-1β, CCL2, and IL-6 were decreased by minocycline i.t. injection (Figures 4K and 4L). To further validate whether S2E could interact with macrophage/microglia directly, we performed immunofluorescence test in SDH collected from a COVID-19 donor and observed obvious co-localization of S2E and IBA1 (Figure 4M). Collectively, these findings indicated that macrophage/microglia were involved in S2E-induced neuroinflammation and pain.

S2E upregulated TLR2 in skin macrophages and spinal microglia

Given that S2E acted as a pathogen-associated molecular pattern which might be recognized by TLRs, we scanned the alteration of TLRs to investigate the innate immunity mechanism of S2E-induced pain. Specifically, we tested the relative expression levels of TLR2, TLR3, TLR4, TLR5, TLR7, and TLR8 in the skin and SDH, as these receptors have been demonstrated to be involved in pain and itch. We found that i.d. injection of S2E upregulated the expression levels of TLR2, TLR4, and TLR8 in the skin from male and female mice, while the expression levels of TLR3, TLR5, and TLR7 were not changed (Figure 5A). Previous study has indicated that TLR2 could sense S2E and then evoked lung inflammation.[30] Therefore, we further examined the protein level of TLR2 in the skin and detected the interaction between TLR2 and S2E. The immunofluorescence results showed that i.d. injection of S2E upregulated the TLR2 protein in male and female mice (Figures 5C and 5D). Since TLR2 is classically known as an innate immune receptor mainly located in macrophages/microglia, we further performed multi-immunofluorescence to verify the interaction between S2E and macrophage TLR2. The results showed the colocalization of S2E (His-tag) and TLR2 were detected in $IBA1^{+}$ macrophages (Figure 5E). These findings suggested a direct interaction of S2E and macrophage TLR2, which might contribute to skin inflammation and pain. Subsequently, we performed this workflow in SDH to investigate the neuroinflammatory effects of S2E in CNS. qPCR results suggested that i.t. injection of S2E upregulated TLR2, TLR4, and TLR8 in male and female mice, consistent with the alteration in the skin (Figure 5B). Next, we applied immunofluorescence analysis to access the protein expression of TLR2 after i.t. injection of S2E. These results indicated that S2E significantly upregulated the protein expression of TLR2 in SDH (Figures 5F and 5G). Moreover, the multi-immunofluorescence showed that TLR2 was mainly located in $IBA1^{+}$ spinal microglia, which was also colocalized with S2E, while tiny S2E signal was detected in $NeuN^{+}$ neurons and $GFAP^{+}$ astrocytes (Figure 5H). The previous results indicated that

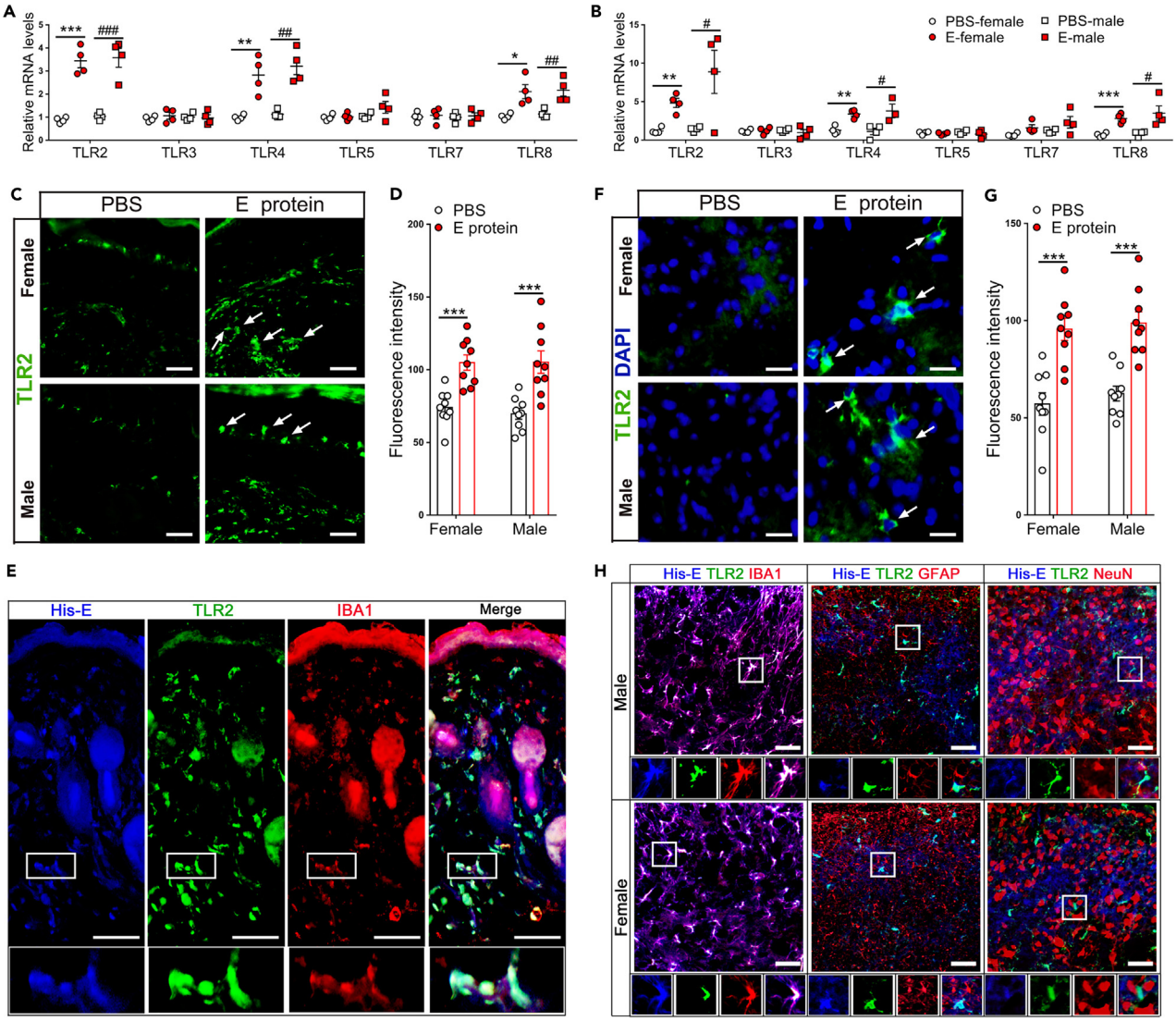

Figure 5. S2E upregulated TLR2 in skin (i.d.) and SDH (i.t.)

(A and B) q-PCR analyzed the expression of TLR2, TLR3, TLR4, TLR5, TLR7, and TLR8 in the skin (A) and SDH (B) of male and female mice. * or $^{\#}p < 0.05$, ** or $^{\#\#}p < 0.01$, *** or $^{\#\#\#}p < 0.001$, Student's t test.

(C and D) Representative images of TLR2 (green) in skin from male and female mice receiving i.d. injection of PBS or S2E (blue for DAPI), along with quantification of TLR2 fluorescence intensity. Scale bar: 50 μm $n = 3$ mice/group. $^{***}p < 0.001$, Student's t test.

(E) Treble-immunostaining showed the overlap of S2E His-tag, TLR2, and IBA1 in the skin from mice receiving i.d. injection of S2E. The enlarged views for the rectangle part were embedded below. Scale bar: 50 μm.

(F and G) Representative images of TLR2 (green) in SDH after i.t. application of S2E (blue for DAPI), along with quantitative analysis. Scale bar: 50 μm.

(H) Treble-immunostaining showed the overlap of S2E His-tag (blue) and TLR2 (green) with IBA1 (red), but not with GFAP (red) (astrocyte marker), and NeuN (red) (neuron marker). The enlarged views for the rectangle part were embedded below. Scale bar: 50 μm.

macrophage/microglia were recognized with S2E via TLR2, potentially leading to the activation of macrophage/microglia inflammatory cascades and subsequent pain symptoms.

S2E triggered microglial neuroinflammation via TLR2-NF-κB signaling *in vitro*

To investigate the role of TLR2 signaling in microglial neuroinflammation induced by S2E, we applied primary microglia culture in conjunction with genetic and pharmacological interference to TLR2. The immunofluorescence results showed that the addition of S2E protein upregulated the expression of TLR2 in IBA1^{+} primary microglia (Figures 6A and 6B). We then analyzed the His-tag signal of S2E within IBA1^{+} region.

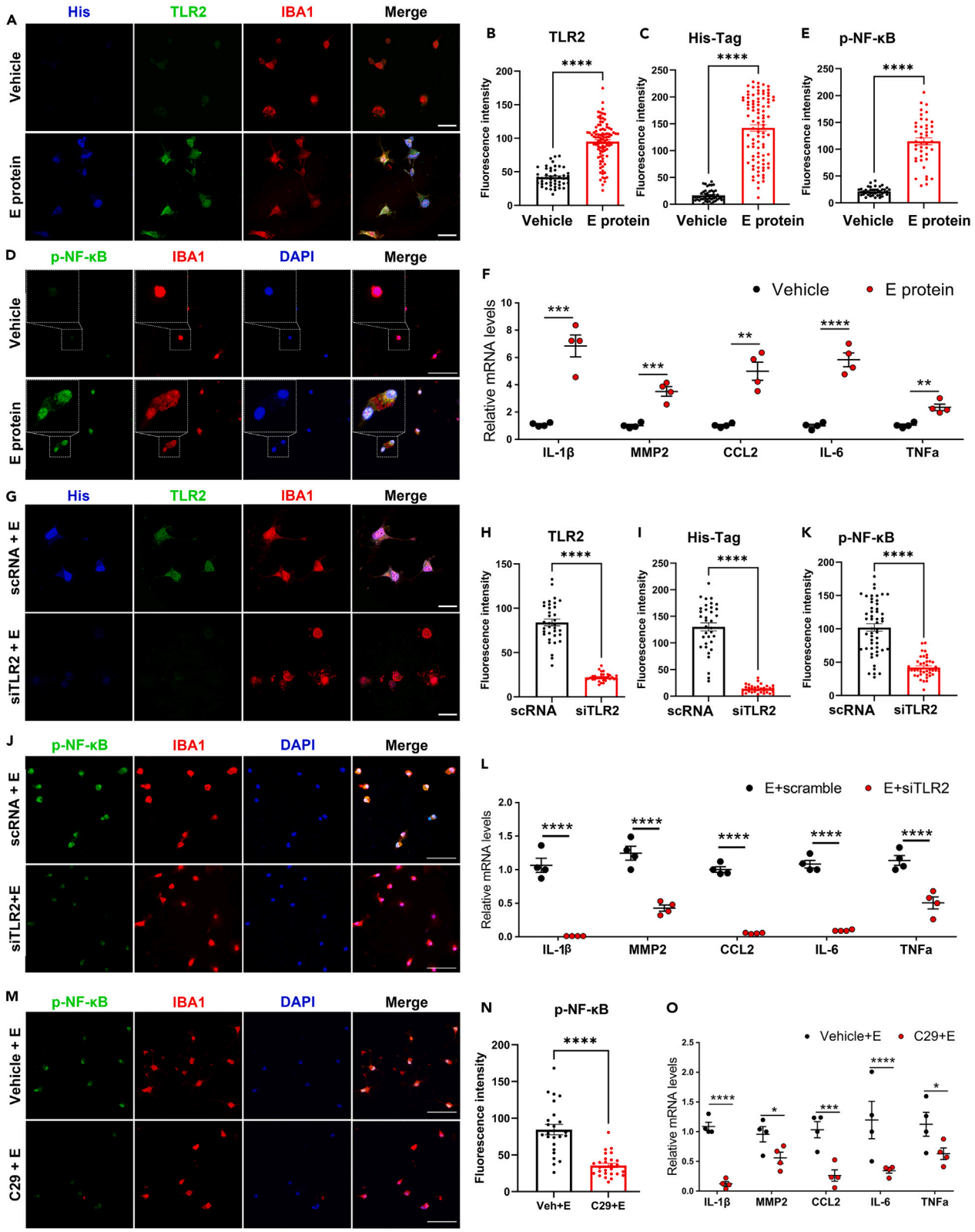
A
His
TLR2
IBA1
Merge
Vehicle
E protein
B
TLR2
Fluorescence intensity
****
Vehicle
E protein
C
His-Tag
****
E
p-NF-κB
****
D
p-NF-κB
IBA1
DAPI
Merge
F
Vehicle
E protein
Relative mRNA levels
***
***
**
****
**
IL-1β
MMP2
CCL2
IL-6
TNFa
G
scRNA + E
siTLR2 + E
H
scRNA
siTLR2
I
K
J
siTLR2+E
L
E+scramble
E+siTLR2
M
Vehicle + E
C29 + E
N
Veh+E
C29+E
O
Vehicle+E
C29+E
*

Figure 6. TLR2 mediated microglia NF-κB activation and neuroinflammation induced by S2E *in vitro*

(A–C) Representative images of microglia stained for His-tag (blue), TLR2 (green), and IBA1 (red) which was cultured with vehicle or S2E, along with quantification of fluorescence intensity for TLR2 and His-tag in IBA1$^+$ area. Scale bar: 20 μm. ****$p < 0.0001$, Student's t test.

(D and E) Representative images of vehicle- or S2E-stimulated microglia stained for p-NF-κB (green) and IBA1 (red) (blue for DAPI), with quantification of p-NF-κB fluorescence intensity. Scale bar: 50 μm ****$p < 0.0001$, Student's t test.

(F) qPCR revealed a significant mRNA upregulation of IL-1β, MMP2, CCL2, IL-6, TNF-α in microglia cultured with S2E. **$p < 0.01$, ***$p < 0.001$, ****$p < 0.0001$, Student's t test.

(G) Immunofluorescence staining of His-tag (blue), TLR2 (green) and IBA1 (red) in scRNA/siTLR2-transfected microglia after stimulation with S2E. Scale bar: 20 μm.

(H and I) Quantification of fluorescence intensity for TLR2 and His-tag in IBA1$^+$ microglia pre-transfected with scRNA or siTLR2. ****$p < 0.0001$, Student's t test.

(J and K) Representative images of microglia stained for p-NF-κB (green) and IBA1 (red) which were cultured with S2E and pre-transferred with scRNA or siTLR2 (blue for DAPI), with quantitative analysis. Scale bar: 50 μm ****$p < 0.0001$, Student's t test.

(L) qPCR revealed a significant downregulation of IL-1β, MMP2, CCL2, IL-6, TNF-α for microglia cultured with S2E and pre-transfected by siTLR2. ****$p < 0.0001$, Student's t test.

(M and N) Immunofluorescence staining of p-NF-κB (green) and IBA1 (red) in microglia stimulated by S2E (blue for DAPI), together with vehicle or C29, along with quantitative analysis. Scale bar: 50 μm ****$p < 0.0001$, Student's t test.

(O) qPCR revealed a downregulated expression of inflammatory factors in S2E-stimulated microglia after C29 treatment. *$p < 0.05$, ***$p < 0.001$, ****$p < 0.0001$, Student's t test.

Notably, increased S2E His-tag signal in IBA1$^+$ microglia was observed as supplying S2E, suggesting that primary microglia could recognize and combine S2E (Figures 6A and 6C). Subsequently, we examined the downstream NF-κB signal in primary microglia as stimulated by S2E. Immunofluorescence results indicated that S2E upregulated the activated phosphorylated form of NF-κB (green), and its fluorescence signal was largely merged with DAPI (blue), a dye for labeling DNA in the nuclear, suggesting the nuclear translocation of p-NF-κB and the subsequent activation of its downstream signaling pathway (Figures 6D and 6E). Moreover, qPCR results indicated that S2E upregulated the mRNA expression of inflammatory factors including IL-1β, MMP2, CCL2, IL-6, and TNFα in primary microglia (Figure 6F).

To further investigate its contribution to S2E-induced microglial neuroinflammation, we employed siRNA interference targeting TLR2 (siTLR2). Compared to control scramble RNA (scRNA), transfection with siTLR2 significantly downregulated the expression of TLR2 in primary microglia (Figures 6G and 6H). Notably, the knockdown of TLR2 also resulted in a significant reduction in the colocalization of S2E and IBA1$^+$ microglia, indicating that microglial TLR2 played a crucial role in the recognition and interaction with S2E (Figures 6G and 6I). Moreover, the activation of NF-κB in primary microglia was decreased by siTLR2, accompanied by a decrease in the expression of inflammatory mediators, including IL-1β, MMP2, CCL2, IL-6, and TNFα (Figures 6J–6L). We also utilized C29, a specific TLR2 inhibitor, to observe its effects on S2E-related microglial neuroinflammation. The immunofluorescence results demonstrated that C29 inhibited the activation of NF-κB induced by S2E in primary microglia (Figures 6M and 6N). Furthermore, qPCR results showed that C29, compared to vehicle, downregulated the expression of neuroinflammatory factors (Figure 6O). These findings collectively suggested that TLR2 mediated the recognition of S2E and activated NF-κB inflammatory pathway in primary microglia.

Macrophage/microglia TLR2 mediated S2E-induced pain

To further investigate whether TLR2 mediated S2E-induced pain, we pre-delivered siRNA by i.d. and i.t. injection to mice receiving S2E and observed its analgesic effects *in vivo* (Figure S9A). Compared to scRNA, siTLR2 significantly downregulated the expression of TLR2 in the skin (i.d.) and SDH (i.t.) (Figures S9B and S9C). Behavioral assessments showed that the knockdown of TLR2 attenuated the mechanical allodynia to 0.4 g von Frey filament and the others (0.16 g, 0.6 g, and 1.0 g), as well as thermal hyperalgesia in the i.d. model (Figures S9D, S9E, and S10A). Additionally, the upregulation of p-NF-κB expression was potently suppressed by siTLR2 (Figures S9H and S6E). For the i.t. model, S2E-induced pain in male and female mice was also markedly inhibited by siTLR2 (Figures S9F, S9G, and S10B), accompanied by a decrease in the expression of p-NF-κB, rather than NF-κB (Figures S9I and S6F). These findings suggested a pivotal role of TLR2 in S2E induced-pain and associated neuroinflammation.

Subsequently, we applied AAV to specifically knockdown TLR2 in macrophage and microglia under the control of Iba1 promoter (Figure 7A). Immunofluorescence tests and western blotting analysis validated the knockdown effectiveness of shTlr2 sequence-loaded virus (AAV2/9-Iba1-zsgreen-shTlr2) which interfered with skin and SDH, compared with NC sequence-loaded virus (AAV2/9-Iba1-zsgreen-NC) (Figures 7B–7E). As expected, behavioral tests indicated that knockdown of TLR2 in macrophage and microglia significantly alleviated the mechanical allodynia and thermal pain induced by S2E, whether administered via i.d. or i.t. injection (Figures 7F–7I, S10C, and S10D). Furthermore, the increased expression of p-NF-κB was obviously downregulated in Iba1-shTlr2 mice, in comparison to the Iba1-NC group (Figures 7J, 7K, S6G, and S6H). Similarly, we also performed von Frey stimuli (0.4g) and Hargreaves tests on *Tlr2* cKO mice and the littermates to observe the S2E-induced mechanical allodynia and thermal hyperalgesia after genetic removing TLR2 in macrophage/microglia using *Cx3cr1* as a specific promoter. The results showed significant alleviations of pain sensations induced by intradermal or intrathecal employment of E protein (Figures 7L–7O).

Additionally, C29 was applied as the specific inhibitor of TLR2 to validate whether pharmacological inhibition would alleviate S2E-induced pain (Figure 8A). For the i.d. model, behavioral assay indicated that co-application of C29 could significantly ameliorate S2E-evoked mechanical allodynia and thermal pain (Figures 8B, 8C, and S11A). Similarly, in the S2E i.t. injection model, co-application of C29, as compared to vehicle, mitigated hypersensitivity to mechanical and heat stimulation in mice injected with S2E (Figures 8D, 8E, and S11B). Moreover, the

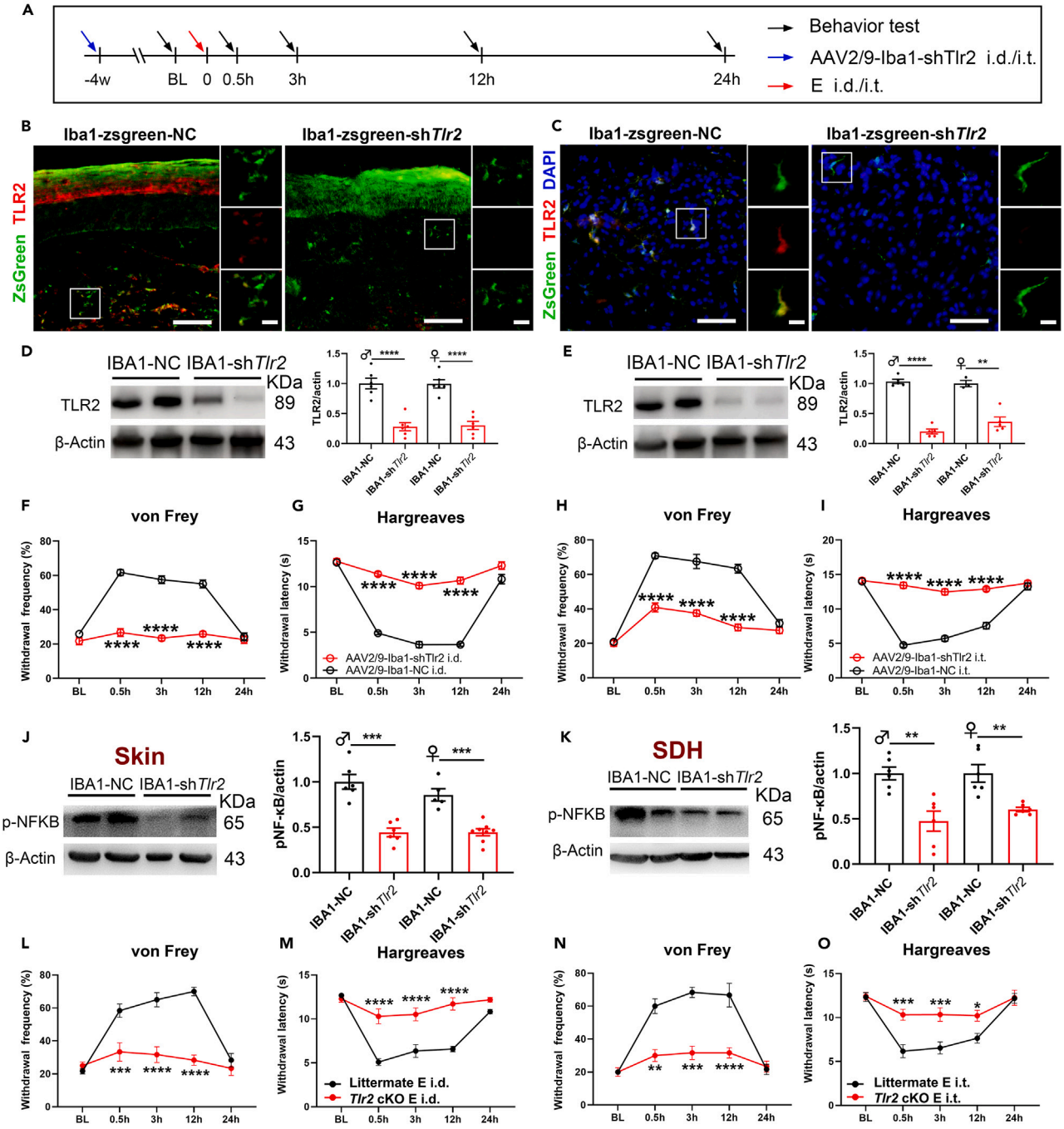

Figure 7. Genetically knocked down of *Tlr2* alleviated S2E evoked pain, and inhibited the activation of p-NF-κB

(A) Timeline of AAV delivery, S2E injection, and behavioral tests.

(B and C) Representative images of ZsGreen (green) and TLR2 (red) immunostaining in skin and SDH from mice infected by AAV (blue for DAPI). Scale bar: 50 μm. The enlarged views for the rectangle part were embedded. Scale bar: 10 μm.

(D and E) Western blotting revealed a significance decrease of TLR2 in the skin and SDH from mice infected by AAV2/9-Iba1-zsgreen-shTlr2, compared with AAV2/9-Iba1-zsgreen-NC. $^{**}p < 0.01$, $^{****}p < 0.0001$, Student's t test.

(F–I) Mechanical allodynia to 0.4 g von Frey filament and thermal hyperalgesia induced by S2E were alleviated by Iba1-sh*Tlr2*. $n = 6$ mice/group in both sexes. $^{****}p < 0.0001$, two-way ANOVA for repeated measures followed by Sidak's post hoc test. (BL: Baseline).

Figure 7. *Continued*

(J and K) Protein level of p-NF-κB in the skin and SDH from AAV-infected mice after S2E application. $^{**}p < 0.01$, $^{***}p < 0.001$, Student's t test.

(L–O) Mechanical allodynia to 0.4 g von Frey filament and thermal hyperalgesia induced by S2E were alleviated by genetic removal of TLR2 in macrophage/microglia. $n = 6$ mice/group in both sexes. $^{*}p < 0.05$, $^{**}p < 0.01$, $^{***}p < 0.001$, $^{****}p < 0.0001$, two-way ANOVA for repeated measures followed by Sidak's post hoc test. (BL: Baseline).

protein level of p-NF-κB in the skin and SDH from mice receiving C29 was determined by western blotting. The analysis of density value of the protein band revealed a significant decrease of p-NF-κB after C29 treatment (Figures 8F, 8G, S6I, and S6J).

DISCUSSION

The extensive pain-related complications in COVID-19 patients indicated the process of SARS-CoV-2 infection and/or other viral elements could initiate nociceptive signaling. In this study, we first demonstrated that membranal protein S2E, rather than S2S or S2M, evoked pain as delivered by i.d. and i.t. injection. We further demonstrated that macrophage/microglia-mediated nociception induced by S2E and that cellular TLR2-NF-κB signaling was responsible for the nociceptive effects of S2E (Figure 9).

Although the World Health Organization has declared that COVID-19 is no longer a global emergency, it is important to note that the pandemic is not yet fully under control. People continue to suffer from post-COVID syndrome, and there are cases of repeated SARS-CoV-2 infections. It has been reported that reinfection of SARS-CoV-2 could further increase additional health risks, such as the sequelae in a broad array of organ systems. Many persistent symptoms reported by individuals who had COVID-19 are related to paraesthesia, such as anosmia, ageusia, joint pain, and myalgia.[38] Moreover, a recent meta-analysis study suggested that neuropathic pain following a COVID-19 infection affected approximately 23.2% of patients,[39] and it was even more common in the case of long COVID syndrome, which was characterized by chronic and debilitating symptoms.[11] Therefore, uncovering the mechanism underlying COVID-related pain symptoms is of paramount importance to alleviate both the acute phase and post-COVID painful experience.

One possible mechanism involves direct viral damage to the central and PNS. Previous studies have indicated that SARS-CoV-2 infection could disrupt the blood-brain barrier (BBB) and subsequently infect the CNS. Additionally, viral proteins produced by SARS-CoV-2, including S2E and S2S, have been shown to directly compromise BBB via a viral infection-independent manner.[40–42] Our immunofluorescence results from human donor samples also suggested that viral proteins could distribute into both the PNS (DRG and TG) and the CNS (SDH). Considering that S2N could hardly contact the surrounding cells, we therefore observed the nociceptive effects of SARS-CoV-2 membranal proteins (S2S, S2M, and S2E) in both i.d. and i.t. models to simulate the peripheral and central effects of these membranal proteins. Among these membranal proteins, only S2E, but not S2S or S2M, evoked pain-like behaviors, which suggested that the membranal proteins of SARS-CoV-2 function distinctly and separately. Particularly, S2S interacted with ACE2 mediating viral entrance to host cells and S2M protected the genetic sequence of SARS-CoV-2, while S2E appeared to trigger inflammatory pathology and pain symptoms.[31] Furthermore, since S2E was a conserved membranal protein found in β-coronavirus, it seemed that its induction of neuroinflammation and pain might also account for the pain complication of others β-coronavirus, such as SARS-CoV, HCoV-HKU1, and MERS-CoV. In addition, the distribution of S2E might include both peripheral organs and nervous system simultaneously, making it important to conduct experiments involving both i.d. and i.t. application of S2E to comprehensively simulate its clinical effects.

It is worth noting that previous studies have indeed demonstrated the pro-inflammatory effects of S2S, while we did not observe its nociceptive effects in neither i.d. nor i.t. application model.[43–45] S2S primarily serves as the key to distinguish ACE2 receptor, which kept in a state of continuous variation for immune escape. Furthermore, it is important to recognize that different SARS-CoV-2 strains might have variations in their effects. The S2S protein used in this study belonged to the Omicron strain which infected the largest populations worldwide. The nociceptive effects of S2S might indeed differ among SARS-CoV-2 strains, and further research is needed to investigate these potential strain-specific variations. However, research involving purified protein components has its limitations in simulating the full spectrum of effects seen during actual virus infections. Therefore, to fully simulate the pain symptom during COVID-19, the intact SARS-CoV-2 virus should be intranasal applied to infect hACE2 transgenic mice.s.

Similarly to most of conditions of chronic pain, SARS-CoV-2 evoked pain exhibits sex dimorphism in clinic. Several prospective/retrospective studies have focused on the sex-related differences, finding that thoracic pain and myalgia occur more frequently in female patients rather than male patients infected by SARS-CoV-2.[46,47] On the contrary, we hardly observed significant differences in pain behavior between male and female mice after S2E injection. One probable mechanism is that chronic pain following SARS-CoV-2 infection is more likely to be influenced by factors such as emotion, hormones, and psychosocial stressors. However, in our study, we only observed acute pain evoked by S2E, which made it difficult to assess long-term effects. Further studies, including longer observation periods, are needed to determine whether the sex difference exists using a SARS-CoV-2 virus infection animal model.

Another advance of this project was uncovering the neuroinflammatory effects of S2E and the role of TLR2 signaling in microglia and macrophage during this process. To verify the pivotal role of microglia/macrophage in this progress, we utilized minocycline as a specific inhibitor. In microglia and macrophages, minocycline reduces the secretion of pro-inflammatory cytokines such as TNF-α, IL-1β, and IL-6, and inhibits the NF-κB signaling pathway, promoting an anti-inflammatory, M2-like phenotype.[36,48–50] As expected, the application of minocycline successfully alleviated the pain behavior and neuroinflammation evoked by S2E. Previous study focused on the pro-inflammatory effects of S2E in lung following systemic application,[29] while we observed that microglia TLR2 could sense S2E both *in vivo* and *in vitro*, leading to characteristic NF-κB associated neuroinflammation. Additionally, apart from TLR2, S2E also upregulated TLR4 and TLR8, the contribution of which to S2E-related pain warrant further investigation.

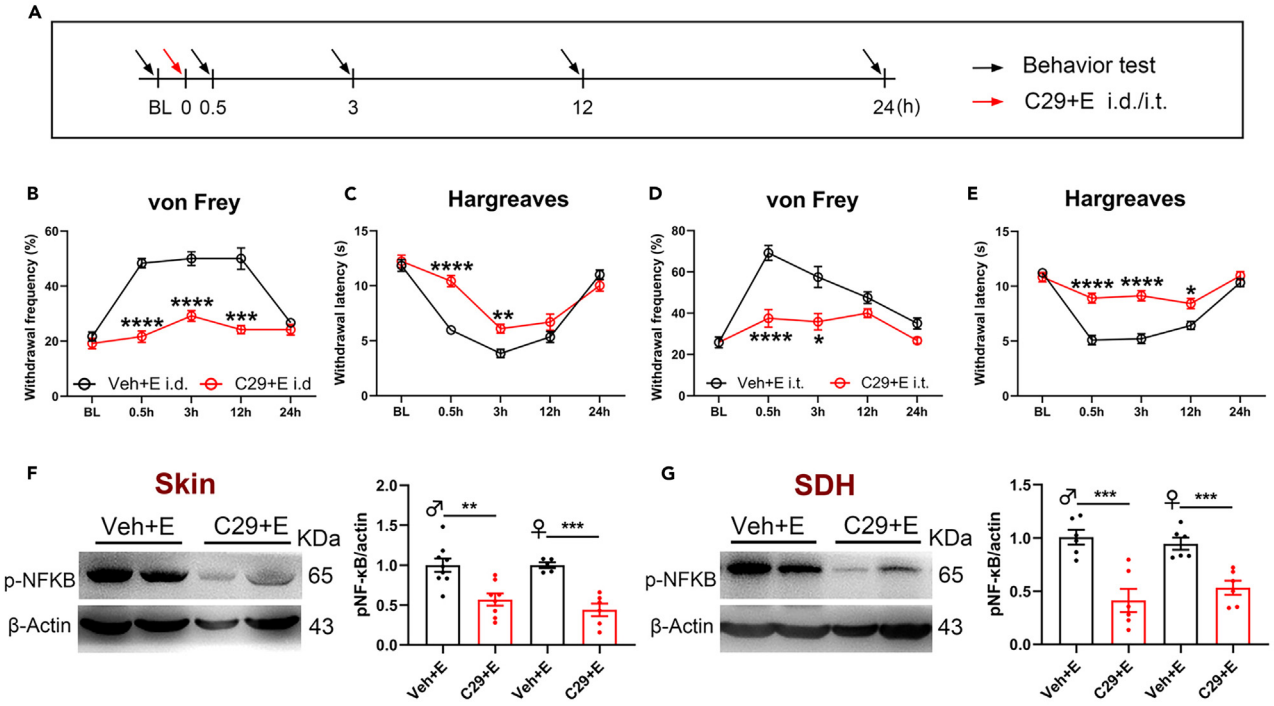

Figure 8. Pharmacological blocking TLR2 mitigated S2E-induced pain and associated neuroinflammation

(A) Timeline of drug delivery, S2E injection, and behavioral tests.

(B–E) Mechanical allodynia to 0.4 g von Frey filament and thermal hyperalgesia induced by S2E were partially mitigated by i.d. or i.t. application of C29. $n = 6$ mice/group in both sexes. $^{*}p < 0.05$, $^{**}p < 0.01$, $^{***}p < 0.001$, $^{****}p < 0.0001$, two-way ANOVA for repeated measures followed by Sidak's post hoc test. (BL: Baseline).

(F) Western blotting analysis of p-NF-κB protein in the skin from mice receiving i.d. co-application of vehicle/C29 and S2E. $^{**}p < 0.01$, $^{***}p < 0.001$, Student's t test.

(G) Western blotting analysis of p-NF-κB protein in SDH from mice receiving i.t. co-application of vehicle/C29 and S2E. $^{**}p < 0.01$, $^{***}p < 0.001$. Student's t test.

Previous study also indicated that microglia ACE2, the receptor for SARS-CoV-2, could mediate the SARS-CoV-2 invasion to microglia and trigger unbalance of Ang II and Ang (1–7), which further contributed to pain.[51–53] Actually, the connection of microglia ACE2 and S2S might facilitate S2E associated neuroinflammation resulting from promoted interaction between microglia TLR2 and S2E. As the classic transcription factor of TLRs signaling, NF-κB gates the release of a range of inflammatory factors and further pathological alterations.[54–56] The present study demonstrated that S2E induced NF-κB nuclear translocation and phosphorylation into the activated form, which was attenuated by genetic knockdown and pharmacological blocking TLR2 in primary culture microglia. In fact, NF-κB activation in microglia under SARS-CoV-2 infection might derive from direct viral infectious process and/or S2E-TLR2 interaction, which remains further research.

An increasing body of evidence suggested that sensory neurons responsible for inducing anosmia are swiftly regulated upon direct interaction with epithelium, to which the virus could readily bind.[22] Similarly, the genesis of pain-like behaviors hinges on the heightened sensitivity of sensory neurons.[57] Our study has elucidated that S2E directly engages with macrophage/microglia TLR2, thereby activating the undergoing NF-κB signaling pathway. This cascade led to the release of inflammatory factors such as IL-1β, IL-6, and CCL2, ultimately sensitizing sensory neurons during the acute pain phase post-injection. Over time, neuronal activity became hyper-sensitive, inactive, or even diminished, culminating in chronic or subdued pain manifestations,[58] a condition colloquially known as long COVID. In fact, our observations indicated that neuroinflammation persists throughout the infection period, encompassing both acute onset and chronic stages. We conducted the tissue collection at the 12 h mark after S2E injection, as this time frame exhibited the most pronounced pain-related behaviors. However, prior research on S2E-induced depression and dysosmia behaviors speculated data collection at 24 h post-injection,[31] with tissue harvested 48 h later. Although the S2E administration protocols differed from ours, it appeared that the induction of inflammation was a consistent finding across various conditions.

Limitations of the study

There are several limitations of this study. First, in our study, S2E only induced acute pain lasting less than 24 h, which did not adequately model the chronic pain associated with COVID-19. Additionally, as a purified protein, S2E cannot fully replicate the complex effects of a SARS-CoV-2 infection. Therefore, further research using SARS-CoV-2 infection animal models with longer observation periods is needed

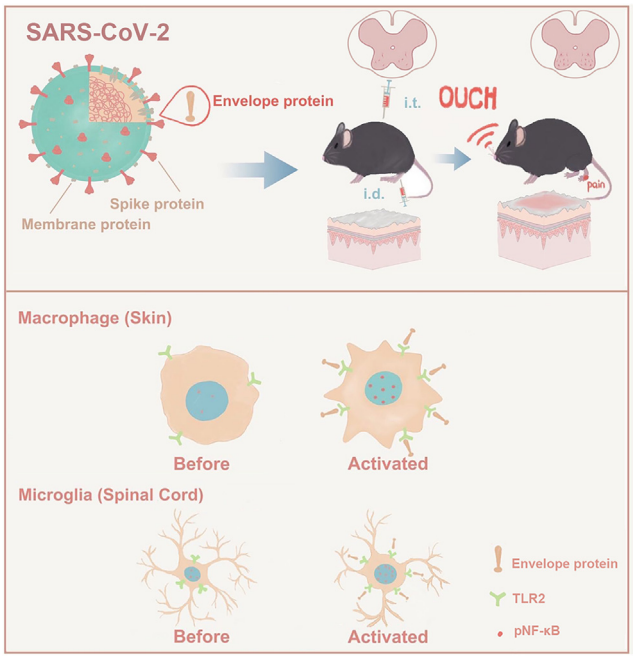

Figure 9. The diagram showed that macrophage/microglia mediated S2E-induced pain via TLR2-NF-κB signaling

to better understand COVID-19 related pain. Second, our assessment of pain was primarily based on evoked pain measures (von Frey and Hargreaves tests), whereas non-stimulus evoked nociception, such as spontaneous pain behaviors (licking, flinching the hind paw), gait analysis, and weight-bearing measures, were not evaluated. These measures can provide a more comprehensive picture of ongoing pain. Moreover, relative emotional behavior tests like sucrose preference test and temperature preference test also make sense to exclude the influence of animal subjective emotional factors.[59] Incorporating these assessments could provide a more accurate evaluation of S2E-evoked pain. Besides, we observed activation of sensory neurons and SDH neurons following S2E injection. This raised the question of whether S2E could directly excite neurons, which warrants further investigation. Lastly, while we attributed the changes caused by intrathecal application of S2E to the interaction with microglial TLR2, macrophages in the DRG might also be affected. This influence could be excluded through more precise genetic regulation of macrophages and microglia, respectively.

RESOURCE AVAILABILITY

Lead contact

Further information and requests for resources and reagents should be directed to and will be fulfilled by lead contact, Chao Ma (machao@ibms.cams.cn).

Materials availability

The study did not generate new unique materials or reagents.

Data and code availability

- This paper does not report nucleotide sequencing-associated datasets, proteomics, peptidomics, metabolomics, structures of biological macromolecules, or small-molecule crystallography.
- This paper does not report original code.
- Any additional information about the data reported in this paper is available from the lead contact upon request.

ACKNOWLEDGMENTS

This study was supported by grants from: STI2030-Major Project #2021ZD0201100 Task 1 #2021ZD0201101, the CAMS Innovation Fund for Medical Sciences (CIFMS #2021-I2M-1-025), and the National Natural Science Foundation of China (82301415).

AUTHOR CONTRIBUTIONS

H.C., F.S., N.Y., and C.M. designed this project. H.C., F.S., and N.Y. drafted the manuscript. H.C., F.S., N.Y., and Y.C. performed the immunofluorescence staining, western blotting, and behavioral test. X.W., Z.C., and N.W. prepared the human tissues. B.Y., P.L., and W.D. helped prepare this manuscript. W.Q., X.Y., and C.M. revised this manuscript. All authors read and approved the final manuscript.

DECLARATION OF INTERESTS

The authors declare no competing interests.

STAR★METHODS

Detailed methods are provided in the online version of this paper and include the following:

- KEY RESOURCES TABLE
- EXPERIMENTAL MODEL AND STUDY PARTICIPANT DETAILS
  - Human sample sources
  - Mouse
  - Primary cell cultures
- METHOD DETAILS
  - Drugs and administration *in vivo*
  - Behavioral tests
  - Primary microglia transfection and drug administration
  - Immunofluorescence staining
  - RNA extraction and quantitative real-time PCR (qPCR)
  - Western blotting
- QUANTIFICATION AND STATISTICAL ANALYSIS

SUPPLEMENTAL INFORMATION

Supplemental information can be found online at https://doi.org/10.1016/j.isci.2024.111027.

Received: May 8, 2024
Revised: June 26, 2024
Accepted: September 20, 2024
Published: September 24, 2024

REFERENCES

1. Guan, W.-j., Ni, Z.-y., Hu, Y., Liang, W.-h., Ou, C.-q., He, J.-x., Liu, L., Shan, H., Lei, C.-l., Hui, D.S.C., et al. (2020). Clinical Characteristics of Coronavirus Disease 2019 in China. N. Engl. J. Med. *382*, 1708–1720. https://doi.org/10.1056/NEJMoa2002032.
2. Solomon, I.H., Normandin, E., Bhattacharyya, S., Mukerji, S.S., Keller, K., Ali, A.S., Adams, G., Hornick, J.L., Padera, R.F., Jr., and Sabeti, P. (2020). Neuropathological Features of Covid-19. N. Engl. J. Med. *383*, 989–992. https://doi.org/10.1056/NEJMc2019373.
3. Mazza, M.G., Palladini, M., De Lorenzo, R., Magnaghi, C., Poletti, S., Furlan, R., Ciceri, F., COVID-19 BioB Outpatient Clinic Study group, Rovere-Querini, P., and Benedetti, F. (2021). Persistent psychopathology and neurocognitive impairment in COVID-19 survivors: Effect of inflammatory biomarkers at three-month follow-up. Brain Behav. Immun. *94*, 138–147. https://doi.org/10.1016/j.bbi.2021.02.021.
4. Mazza, M.G., De Lorenzo, R., Conte, C., Poletti, S., Vai, B., Bollettini, I., Melloni, E.M.T., Furlan, R., Ciceri, F., Rovere-Querini, P., et al. (2020). Anxiety and depression in COVID-19 survivors: Role of inflammatory and clinical predictors. Brain Behav. Immun. *89*, 594–600. https://doi.org/10.1016/j.bbi.2020.07.037.
5. Buckley, L., Sterling, M., and Elphinston, R.A. (2023). Chronic pain experience through COVID-19: a comparison of reports prior and during the early stages of the pandemic. Pain *164*, 435–442.
6. Krajewski, P.K., Szepietowski, J.C., and Maj, J. (2020). Cutaneous hyperesthesia: A novel manifestation of COVID-19. Brain Behav. Immun. *87*, 188. https://doi.org/10.1016/j.bbi.2020.05.064.
7. Avula, A., Nalleballe, K., Narula, N., Sapozhnikov, S., Dandu, V., Toom, S., Glaser, A., and Elsayegh, D. (2020). COVID-19 presenting as stroke. Brain Behav. Immun. *87*, 115–119. https://doi.org/10.1016/j.bbi.2020.04.077.
8. Zheng, J., Wong, L.Y.R., Li, K., Verma, A.K., Ortiz, M.E., Wohlford-Lenane, C., Leidinger, M.R., Knudson, C.M., Meyerholz, D.K., McCray, P.B., Jr., and Perlman, S. (2021). COVID-19 treatments and pathogenesis including anosmia in K18-hACE2 mice. Nature *589*, 603–607. https://doi.org/10.1038/s41586-020-2943-z.
9. Wu, Y., Xu, X., Chen, Z., Duan, J., Hashimoto, K., Yang, L., Liu, C., and Yang, C. (2020). Nervous system involvement after infection with COVID-19 and other coronaviruses. Brain Behav. Immun. *87*, 18–22. https://doi.org/10.1016/j.bbi.2020.03.031.
10. Matschke, J., Lütgehetmann, M., Hagel, C., Sperhake, J.P., Schröder, A.S., Edler, C., Mushumba, H., Fitzek, A., Allweiss, L., Dandri, M., et al. (2020). Neuropathology of patients with COVID-19 in Germany: a post-mortem case series. Lancet Neurol. *19*, 919–929. https://doi.org/10.1016/s1474-4422(20)30308-2.
11. Shanthanna, H., Nelson, A.M., Kissoon, N., and Narouze, S. (2022). The COVID-19 pandemic and its consequences for chronic pain: a narrative review. Anaesthesia *77*, 1039–1050. https://doi.org/10.1111/anae.15801.
12. Fernández-de-las-Peñas, C., Cancela-Cilleruelo, I., Moro-López-Menchero, P., Rodríguez-Jiménez, J., Pellicer-Valero, O.J., Martín-Guerrero, J.D., and Arendt-Nielsen, L. (2023). Exploring the trajectory curve of long-term musculoskeletal post-COVID pain symptoms in hospitalized COVID-19 survivors: a multicenter study. Pain *164*, 413.
13. Fernández-de-las-Peñas, C., de-la-Llave-Rincón, A.I., Ortega-Santiago, R., Ambite-Quesada, S., Gómez-Mayordomo, V., Cuadrado, M.L., Arias-Navalón, J.A., Hernández-Barrera, V., Martín-Guerrero, J.D., Pellicer-Valero, O.J., and Arendt-Nielsen, L. (2022). Prevalence and risk factors of musculoskeletal pain symptoms as long-term post-COVID sequelae in hospitalized COVID-19 survivors: a multicenter study. Pain *163*, e989.
14. Kurçaloğlu, M., Bilek, H.C., Erbaş, S.N., Özkan, F., Tanyel, E., Deveci, A., Ketenci, S., and Güldoğuş, F. (2021). Evaluation of pain in patients with COVID-19. Agri : Agri (Algoloji) Dernegi'nin Yayin organidir = J. Turkish Soc. Algol. *33*, 215–222. https://doi.org/10.14744/agri.2021.92609.
15. Tana, C., Bentivegna, E., Cho, S.J., Harriott, A.M., García-Azorín, D., Labastida-Ramirez, A., Ornello, R., Raffaelli, B., Beltrán, E.R., Ruscheweyh, R., and Martelletti, P. (2022). Long COVID headache. J. Headache Pain *23*, 93. https://doi.org/10.1186/s10194-022-01450-8.
16. Ballering, A.V., van Zon, S.K.R., Olde Hartman, T.C., and Rosmalen, J.G.M.; Lifelines Corona Research Initiative (2022). Persistence of somatic symptoms after COVID-19 in the Netherlands: an observational cohort study. Lancet *400*, 452–461. https://doi.org/10.1016/s0140-6736(22)01214-4.
17. Aksan, F., Nelson, E.A., and Swedish, K.A. (2020). A COVID-19 patient with intense burning pain. J. Neurovirol. *26*, 800–801. https://doi.org/10.1007/s13365-020-00887-4.
18. Davis, H.E., McCorkell, L., Vogel, J.M., and Topol, E.J. (2023). Long COVID: major findings, mechanisms and recommendations. Nat. Rev. Microbiol. *21*, 133–146. https://doi.org/10.1038/s41579-022-00846-2.
19. Song, E., Zhang, C., Israelow, B., Lu-Culligan, A., Prado, A.V., Skriabine, S., Lu, P., Weizman,

O.E., Liu, F., Dai, Y., et al. (2021). Neuroinvasion of SARS-CoV-2 in human and mouse brain. J. Exp. Med. *218*, e20202135. https://doi.org/10.1084/jem.20202135.
20. Luis, M.B., Liguori, N.F., López, P.A., and Alonso, R. (2021). SARS-CoV-2 RNA detection in cerebrospinal fluid: Presentation of two cases and review of literature. Brain Behav. Immun. Health *15*, 100282. https://doi.org/10.1016/j.bbih.2021.100282.
21. Vanderheiden, A., and Klein, R.S. (2022). Neuroinflammation and COVID-19. Curr. Opin. Neurobiol. *76*, 102608. https://doi.org/10.1016/j.conb.2022.102608.
22. Song, W.J., Hui, C.K.M., Hull, J.H., Birring, S.S., McGarvey, L., Mazzone, S.B., and Chung, K.F. (2021). Confronting COVID-19-associated cough and the post-COVID syndrome: role of viral neurotropism, neuroinflammation, and neuroimmune responses. Lancet Respir. Med. *9*, 533–544. https://doi.org/10.1016/s2213-2600(21)00125-9.
23. Wang, M.Y., Zhao, R., Gao, L.J., Gao, X.F., Wang, D.P., and Cao, J.M. (2020). SARS-CoV-2: Structure, Biology, and Structure-Based Therapeutics Development. Front. Cell. Infect. Microbiol. *10*, 587269. https://doi.org/10.3389/fcimb.2020.587269.
24. Cao, Y., Yang, R., Lee, I., Zhang, W., Sun, J., Wang, W., and Meng, X. (2021). Characterization of the SARS-CoV-2 E Protein: Sequence, Structure, Viroporin, and Inhibitors. Protein Sci. *30*, 1114–1130. https://doi.org/10.1002/pro.4075.
25. Schoeman, D., and Fielding, B.C. (2019). Coronavirus envelope protein: current knowledge. Virol. J. *16*, 69. https://doi.org/10.1186/s12985-019-1182-0.
26. Benameur, K., Agarwal, A., Auld, S.C., Butters, M.P., Webster, A.S., Ozturk, T., Howell, J.C., Bassit, L.C., Velasquez, A., Schinazi, R.F., et al. (2020). Encephalopathy and Encephalitis Associated with Cerebrospinal Fluid Cytokine Alterations and Coronavirus Disease, Atlanta, Georgia, USA, 2020. Emerg. Infect. Dis. *26*, 2016–2021. https://doi.org/10.3201/eid2609.202122.
27. Nuovo, G.J., Magro, C., and Mikhail, A. (2020). Cytologic and molecular correlates of SARS-CoV-2 infection of the nasopharynx. Ann. Diagn. Pathol. *48*, 151565. https://doi.org/10.1016/j.anndiagpath.2020.151565.
28. Magro, C.M., Mulvey, J., Kubiak, J., Mikhail, S., Suster, D., Crowson, A.N., Laurence, J., and Nuovo, G. (2021). Severe COVID-19: A multifaceted viral vasculopathy syndrome. Ann. Diagn. Pathol. *50*, 151645. https://doi.org/10.1016/j.anndiagpath.2020.151645.
29. Xia, B., Shen, X., He, Y., Pan, X., Liu, F.L., Wang, Y., Yang, F., Fang, S., Wu, Y., Duan, Z., et al. (2021). SARS-CoV-2 envelope protein causes acute respiratory distress syndrome (ARDS)-like pathological damages and constitutes an antiviral target. Cell Res. *31*, 847–860. https://doi.org/10.1038/s41422-021-00519-4.
30. Zheng, M., Karki, R., Williams, E.P., Yang, D., Fitzpatrick, E., Vogel, P., Jonsson, C.B., and Kanneganti, T.D. (2021). TLR2 senses the SARS-CoV-2 envelope protein to produce inflammatory cytokines. Nat. Immunol. *22*, 829–838. https://doi.org/10.1038/s41590-021-00937-x.
31. Su, W., Ju, J., Gu, M., Wang, X., Liu, S., Yu, J., and Mu, D. (2023). SARS-CoV-2 envelope protein triggers depression-like behaviors and dysosmia via TLR2-mediated neuroinflammation in mice. J. Neuroinflammation *20*, 110. https://doi.org/10.1186/s12974-023-02786-x.
32. Bonhomme, D., Cavaillon, J.M., and Werts, C. (2024). The dangerous liaisons in innate immunity involving recombinant proteins and endotoxins: Examples from the literature and the Leptospira field. J. Biol. Chem. *300*, 105506. https://doi.org/10.1016/j.jbc.2023.105506.
33. Woller, S.A., Ravula, S.B., Tucci, F.C., Beaton, G., Corr, M., Isseroff, R.R., Soulika, A.M., Chigbrow, M., Eddinger, K.A., and Yaksh, T.L. (2016). Systemic TAK-242 prevents intrathecal LPS evoked hyperalgesia in male, but not female mice and prevents delayed allodynia following intraplantar formalin in both male and female mice: The role of TLR4 in the evolution of a persistent pain state. Brain Behav. Immun. *56*, 271–280. https://doi.org/10.1016/j.bbi.2016.03.026.
34. Gyimesi, E., Gönczi, F., Szilasi, M., Pál, G., Baráth, S., and Sipka, S. (2013). The effects of various doses of bacterial lipopolysaccharide on the expression of CD63 and the release of histamine by basophils of atopic and non-atopic patients. Inflamm. Res. *62*, 213–218. https://doi.org/10.1007/s00011-012-0569-9.
35. Utz, S.G., See, P., Mildenberger, W., Thion, M.S., Silvin, A., Lutz, M., Ingelfinger, F., Rayan, N.A., Lelios, I., Buttgereit, A., et al. (2020). Early Fate Defines Microglia and Non-parenchymal Brain Macrophage Development. Cell *181*, 557–573.e18. https://doi.org/10.1016/j.cell.2020.03.021.
36. Kobayashi, K., Imagama, S., Ohgomori, T., Hirano, K., Uchimura, K., Sakamoto, K., Hirakawa, A., Takeuchi, H., Suzumura, A., Ishiguro, N., and Kadomatsu, K. (2013). Minocycline selectively inhibits M1 polarization of microglia. Cell Death Dis. *4*, e525. https://doi.org/10.1038/cddis.2013.54.
37. Li, Y., Zhang, Z., Xu, K., Du, S., Gu, X., Cao, R., and Cui, S. (2021). Minocycline alleviates peripheral nerve adhesion by promoting regulatory macrophage polarization via the TAK1 and its downstream pathway. Life Sci. *276*, 119422. https://doi.org/10.1016/j.lfs.2021.119422.
38. Mizrahi, B., Sudry, T., Flaks-Manov, N., Yehezkelli, Y., Kalkstein, N., Akiva, P., Ekka-Zohar, A., Ben David, S.S., Lerner, U., Bivas-Benita, M., and Greenfeld, S. (2023). Long covid outcomes at one year after mild SARS-CoV-2 infection: nationwide cohort study. Bmj *380*, e072529. https://doi.org/10.1136/bmj-2022-072529.
39. Topal, İ., Özçelik, N., and Atayoğlu, A.T. (2022). Post-COVID-19 pain syndrome: a descriptive study in Turkish population. Korean J. Pain *35*, 468–474. https://doi.org/10.3344/kjp.2022.35.4.468.
40. Ju, J., Su, Y., Zhou, Y., Wei, H., and Xu, Q. (2022). The SARS-CoV-2 envelope protein disrupts barrier function in an in vitro human blood-brain barrier model. Front. Cell. Neurosci. *16*, 897564. https://doi.org/10.3389/fncel.2022.897564.
41. Krasemann, S., Haferkamp, U., Pfefferle, S., Woo, M.S., Heinrich, F., Schweizer, M., Appelt-Menzel, A., Cubukova, A., Barenberg, J., Leu, J., et al. (2022). The blood-brain barrier is dysregulated in COVID-19 and serves as a CNS entry route for SARS-CoV-2. Stem Cell Rep. *17*, 307–320. https://doi.org/10.1016/j.stemcr.2021.12.011.
42. Chen, Y., Yang, W., Chen, F., and Cui, L. (2022). COVID-19 and cognitive impairment: neuroinvasive and blood–brain barrier dysfunction. J. Neuroinflammation *19*, 222. https://doi.org/10.1186/s12974-022-02579-8.
43. Frank, M.G., Nguyen, K.H., Ball, J.B., Hopkins, S., Kelley, T., Baratta, M.V., Fleshner, M., and Maier, S.F. (2022). SARS-CoV-2 spike S1 subunit induces neuroinflammatory, microglial and behavioral sickness responses: Evidence of PAMP-like properties. Brain Behav. Immun. *100*, 267–277. https://doi.org/10.1016/j.bbi.2021.12.007.
44. Alves, V.S., Santos, S.A.C.S., Leite-Aguiar, R., Paiva-Pereira, E., Dos Reis, R.R., Calazans, M.L., Fernandes, G.G., Antônio, L.S., de Lima, E.V., Kurtenbach, E., et al. (2023). SARS-CoV-2 Spike protein alters microglial purinergic signaling. Front. Immunol. *14*, 1158460. https://doi.org/10.3389/fimmu.2023.1158460.
45. Fontes-Dantas, F.L., Fernandes, G.G., Gutman, E.G., De Lima, E.V., Antonio, L.S., Hammerle, M.B., Mota-Araujo, H.P., Colodeti, L.C., Araújo, S.M.B., Froz, G.M., et al. (2023). SARS-CoV-2 Spike protein induces TLR4-mediated long-term cognitive dysfunction recapitulating post-COVID-19 syndrome in mice. Cell Rep. *42*, 112189. https://doi.org/10.1016/j.celrep.2023.112189.
46. Pelà, G., Goldoni, M., Solinas, E., Cavalli, C., Tagliaferri, S., Ranzieri, S., Frizzelli, A., Marchi, L., Mori, P.A., Majori, M., et al. (2022). Sex-Related Differences in Long-COVID-19 Syndrome. J. Womens Health *31*, 620–630. https://doi.org/10.1089/jwh.2021.0411.
47. Cho, S.M., Premraj, L., Battaglini, D., Fanning, J.P., Suen, J., Bassi, G.L., Fraser, J., Robba, C., Griffee, M., Solomon, T., et al. (2024). Sex differences in post-acute neurological sequelae of SARS-CoV-2 and symptom resolution in adults after coronavirus disease 2019 hospitalization: an international multi-centre prospective observational study. Brain Commun. *6*, fcae036. https://doi.org/10.1093/braincomms/fcae036.
48. Blecharz-Lang, K.G., Patsouris, V., Nieminen-Kelhä, M., Seiffert, S., Schneider, U.C., and Vajkoczy, P. (2022). Minocycline Attenuates Microglia/Macrophage Phagocytic Activity and Inhibits SAH-Induced Neuronal Cell Death and Inflammation. Neurocrit. Care *37*, 410–423. https://doi.org/10.1007/s12028-022-01511-5.
49. Lopes, F.S.R., Giardini, A.C., Sant'Anna, M.B., Kimura, L.F., Bufalo, M.C., Vigerelli, H., Zambelli, V.O., and Picolo, G. (2022). Crotalphine Modulates Microglia M1/M2 Phenotypes and Induces Spinal Analgesia Mediated by Opioid-Cannabinoid Systems. Int. J. Mol. Sci. *23*, 11571. https://doi.org/10.3390/ijms231911571.
50. Lee, J.Y., Park, C.S., Seo, K.J., Kim, I.Y., Han, S., Youn, I., and Yune, T.Y. (2023). IL-6/JAK2/STAT3 axis mediates neuropathic pain by regulating astrocyte and microglia activation after spinal cord injury. Exp. Neurol. *370*, 114576. https://doi.org/10.1016/j.expneurol.2023.114576.
51. Su, S., Cui, H., Wang, T., Shen, X., and Ma, C. (2020). Pain: A potential new label of COVID-19. Brain Behav. Immun. *87*, 159–160. https://doi.org/10.1016/j.bbi.2020.05.025.
52. Nemoto, W., Nakagawasai, O., Yaoita, F., Kanno, S.I., Yomogida, S., Ishikawa, M., Tadano, T., and Tan-No, K. (2013). Angiotensin II produces nociceptive behavior through spinal AT1 receptor-mediated p38 mitogen-activated protein kinase activation in mice. Mol. Pain *9*, 38. https://doi.org/10.1186/1744-8069-9-38.

53. Yamagata, R., Nemoto, W., Nakagawasai, O., Takahashi, K., and Tan-No, K. (2020). Downregulation of spinal angiotensin converting enzyme 2 is involved in neuropathic pain associated with type 2 diabetes mellitus in mice. Biochem. Pharmacol. *174*, 113825. https://doi.org/10.1016/j.bcp.2020.113825.
54. Yang, H., Wu, L., Deng, H., Chen, Y., Zhou, H., Liu, M., Wang, S., Zheng, L., Zhu, L., and Lv, X. (2020). Anti-inflammatory protein TSG-6 secreted by bone marrow mesenchymal stem cells attenuates neuropathic pain by inhibiting the TLR2/MyD88/NF-κB signaling pathway in spinal microglia. J. Neuroinflammation *17*, 154. https://doi.org/10.1186/s12974-020-1731-x.
55. Shen, J., Fang, J., Hao, J., Zhong, X., Wang, D., Ren, H., and Hu, Z. (2016). SIRT1 Inhibits the Catabolic Effect of IL-1β Through TLR2/SIRT1/NF-κB Pathway in Human Degenerative Nucleus Pulposus Cells. Pain Physician *19*, E215–E226.
56. Xie, W., Wang, Y., Huang, Y., Yang, H., Wang, J., and Hu, Z. (2009). Toll-like receptor 2 mediates invasion via activating NF-kappaB in MDA-MB-231 breast cancer cells. Biochem. Biophys. Res. Commun. *379*, 1027–1032. https://doi.org/10.1016/j.bbrc.2009.01.009.
57. Gracely, R.H., Undem, B.J., and Banzett, R.B. (2007). Cough, pain and dyspnoea: similarities and differences. Pulm. Pharmacol. Ther. *20*, 433–437. https://doi.org/10.1016/j.pupt.2006.12.005.
58. Coen, M., Kaiser, C., Naimi, R., Uginet, M., Hentsch, L., Serratrice, J., and Allali, G. (2021). Beyond silent hypoxemia: Does COVID-19 can blunt pain perception? Comment on "The neuroinvasive potential of SARS CoV2 may play a role in the respiratory failure of COVID 19 patients. J. Med. Virol. *93*, 1915–1916. https://doi.org/10.1002/jmv.26753.
59. Deuis, J.R., Dvorakova, L.S., and Vetter, I. (2017). Methods Used to Evaluate Pain Behaviors in Rodents. Front. Mol. Neurosci. *10*, 284. https://doi.org/10.3389/fnmol.2017.00284.
60. Leng, L., Zhuang, K., Liu, Z., Huang, C., Gao, Y., Chen, G., Lin, H., Hu, Y., Wu, D., Shi, M., et al. (2018). Menin Deficiency Leads to Depressive-like Behaviors in Mice by Modulating Astrocyte-Mediated Neuroinflammation. Neuron *100*, 551–563.e7. https://doi.org/10.1016/j.neuron.2018.08.031.

STAR★METHODS

KEY RESOURCES TABLE

REAGENT or RESOURCE	SOURCE	IDENTIFIER
Antibodies		
Rabbit monoclonal anti-TLR2	Abcam	Cat#: ab209216
Mouse anti-His-tag	MBL	Cat#: D291-3; RRID: AB_10597733
Goat polyclonal anti-IBA1	Abcam	Cat#: ab5076; RRID: AB_2224402
Chicken polyclonal anti-GFAP	Abcam	Cat#: ab4674; RRID: AB_304558
Mouse monoclonal anti-NeuN	Abcam	Cat#: ab104224; RRID: AB_10711040
Mouse monoclonal anti-*c*-Fos	Abcam	Cat#: ab208942; RRID: AB_2747772
Rabbit anti-*p*-ERK	Cell Signaling Technology	Cat#: 4370; RRID: AB_2315112
Rabbit anti-S2E	Proteintech	Cat#: 28904; RRID: AB_2881232
Rabbit anti-S2S	GeneTex	Cat#: GTX635654; RRID: AB_2888548
Rabbit anti-S2M	GeneTex	Cat#: GTX636245; RRID: AB_2909954
Rabbit monoclonal isotype IgG	Cell Signaling Technology	Cat#: 3900; RRID: AB_1550038
Donkey anti-mouse Alexa 405	Abcam	Cat#: ab175658; RRID: AB_2687445
Donkey anti-rabbit Alexa 488	Abcam	Cat#: ab150073; RRID: AB_2636877
Donkey anti-rabbit Alexa 594	Invitrogen	Cat#: A-21207; RRID: AB_
Donkey anti-mouse Alexa 594	Abcam	Cat#: ab150108; RRID: AB_2732073
Donkey anti-goat Alexa 594	Abcam	Cat#: ab150132; RRID: AB_2810222
Goat anti-chicken Alexa 594	Abcam	Cat#: ab150176; RRID: AB_2716250
Rabbit anti NF-κB	Cell Signaling Technology	Cat#: 8242; RRID: AB_10859369
Rabbit anti-p-NF-κB (Ser536)	Cell Signaling Technology	Cat#: 3033; RRID: AB_331284
Mouse anti-β-Actin	Cell Signaling Technology	Cat#: 3700; RRID: AB_2242334
Anti-mouse HRP-linked antibody	Cell Signaling Technology	Cat#: 7076; RRID: AB_330924
Anti-rabbit HRP-linked antibody	Cell Signaling Technology	Cat#: 7074; RRID: AB_2099233
Chemicals, peptides, and recombinant proteins		
S2E protein	Acro Biosystems	Cat#: ENN-C5128
S2M protein	Prosci	Cat#: 10-429
S2S protein (Omicron B.1.1.529)	Sino Biological	Cat#: 40591-V08H41
Minocycline	Sigma-Aldrich	Cat#: M9511 CAS: 13614-98-7
C29	Med Chem Express	Cat#: HY-100461
Polymyxin B	Med Chem Express	Cat#: HY-149179
Lipocat3000	Aoqing Biotechnology	Cat#: AQ11668 Lot#: 668050322
Critical commercial assays		
PFA	Biotopped	Cat#: Top0382
TRIzol	Invitrogen	Lot#: 99088501 REF#: 15596018CN
T-PER™ tissue protein extraction reagent	Thermo Stientific	Cat#: 78510
PrimeScript™ RT Master Mix	Takara	Cat#: RR036A
MagicSYBR Mixture	Cwbio	Cat#: CW3008
Chromogenic LAL Endotoxin Assay Kit	Beyotime	Cat#: C0276S
eECL western blot kit	Tanon	Cat#: 180-5001

(*Continued on next page*)

Continued

REAGENT or RESOURCE	SOURCE	IDENTIFIER
Experimental models: organisms/strains		
Mouse: *Tlr2*$^{flox/flox}$	GemPharmatech	N/A
Mouse: *Cx3cr1*$^{cre/+}$	GemPharmatech	N/A
Virus: AAV2/9-Iba1-zsgreen-*sh*Tlr2	HanBio	N/A
Virus: AAV2/9-Iba1-zsgreen-NC	HanBio	N/A
Oligonucleotides		
Primers for qPCR	This paper	Table S2
siRNA targeting *Tlr2*	KeyGen Biotech	R206071341/1342
Nontargeting scrambled controls	KeyGen Biotech	N/A
Software and algorithms		
SPSS (version 17.0)	IBM	https://www.ibm.com/cn-zh/products/spss-statistics
Prism 9	Graphpad	https://www.graphpad.com/scientific-software/prism/
FluoView	Olympus	N/A
Other		
Video Camera	SONY	HDT-PJ580E
Real-time PCR Detection system	BioRad	CFX96
Western blot imaging system	Cytiva	Amersham ImageQuant 800
Laser confocal microscopic imaging system	Olympus	FV1000
Laser confocal microscopic imaging system	Leica	TCS-SP8 STED 3×

EXPERIMENTAL MODEL AND STUDY PARTICIPANT DETAILS

Human sample sources

The lung, spinal cord, DRG and TG samples were recruited from the National Human Brain Bank for Development and Function, Chinese Academy of Medical Sciences, and Peking Union Medical College (PUMC) in Beijing, China. The COVID-19 medical history was reported by donors' dependent. Detailed information of all the donors was listed in Table S1. The research protocol was approved by the Institutional Review Board of the Institute of Basic Medical Sciences of the Chinese Academy of Medical Sciences, PUMC, Beijing, China (approval number: 2022125).

Mouse

Wild type C57BL/6J adult male and female mice (20–24 g) were both used in this study. Mice were housed under a controlled room (23±3°C, 12-h light/12-h dark cycle) with *ad libitum* access to a standard diet and water. All protocols were approved by the Institutional Animal Care and Use Committee in the Chinese Academy of Medical Sciences, Institute of Basic Medical Sciences (approval number: #211-2014). Mice were randomly assigned to experimental groups.

Tlr2$^{fl/fl}$ and *Cx3cr1-Cre*$^{+/-}$ mice were purchased in GemPharmatech LLC. (Jiangsu, China). *Tlr2*$^{fl/fl}$: *Cx3cr1-Cre* conditional knockout mice (cKO-macrophage/microglia) were generated by crossing *Tlr2*$^{fl/fl}$ with *Cx3cr1-Cre*$^{+/-}$ mice to generate the heterozygotes *Tlr2*$^{fl/-}$: *Cx3cr1-Cre* and then crossed with *Tlr2*$^{fl/fl}$ mice. The *Tlr2*$^{fl/fl}$: *Cx3cr1-Cre*$^{-/-}$ mice were selected to be littermates.

Primary cell cultures

Pure neonatal microglia were obtained from the cortices of neonatal C57BL/6J mice (P1-P3) as previously described.[60] In brief, the cortices were stripped of meninges and collected in DMEM medium containing 1.0% penicillin/streptomycin and dissociated by repeated up- and down-pipetting. The resulting cell suspension was centrifuged at 1200 rpm for 3 min. Cells were re-suspended in DMEM medium with 10% FBS and 1% penicillin/streptomycin, which were cultured at 37°C with 5% CO_2. To harvest pure microglia from this initial co-culture, culture flasks were shaken for 1 h on a homo-thermal shaker (37°C, 200 rpm) to detach microglia. The medium containing detached microglia was collected and immediately centrifuged for 2 min at 1200 rpm. The supernatant was removed, and the obtained pure microglia pellet was re-suspended in fresh culture medium and then seeded into subcultures. Microglia harvesting was repeated for maximally three times at intervals of 3 days. All experiments were performed with these purified microglia cultures.

METHOD DETAILS

Drugs and administration *in vivo*

S2E protein (Acro Biosystems, ENN-C5128, China) was prepared in PBS (0.01, 0.1 and 1 mg/mL) and delivered 10 μL for each mouse. S2M protein (Prosci, 10-429, USA) and S2S protein (Sino Biological, 40591-V08H41, Omicron B.1.1.529, China) were prepared in PBS (0.1 mg/mL) and delivered 10 μL for each mouse. The microglia inhibitor minocycline (M9511, Sigma-Aldrich, USA) was prepared in PBS (1.0 mg/mL) and delivered 10 μL for each mouse 2 days prior to S2E injection. The TLR2 inhibitor C29 was obtained from Med Chem Express (HY-100461, China) and dissolved in PBS containing 10% DMSO (100mM for behavior test and 100 μM for *in vitro* test). For *in vitro* study, the siRNA targeting TLR2 (siTLR2, 50 nM, KeyGen Biotech, Jiangsu, China) or nontargeting scrambled controls (scRNA, 50 nM, KeyGen Biotech, Jiangsu, China) was applied by Lipocat3000 transfection reagent (Aoqing Biotechnology, Beijing, China). For behavior assay, siTLR2 (0.5 μg/μL) or scRNA (0.5 μg/μL) was dissolved in PBS solution prepared with RNase-free water.

Polymyxin B (PMB) was applied to neutralize the potential lipopolysaccharide (LPS) in commercial S2E purified from *E.coli*. Briefly, the PMB (Med Chem Express, HY-149179, China) was dissolved in PBS (250 μg/mL) and was pre-incubation with S2E (0.1 μg/μL) at 37°C for 1 h before injection.

Intradermal injection was performed under short-term anesthesia with isoflurane. Drugs were subcutaneously injected into the plantar hind paw by insulin syringe. Intrathecal injection was performed by an insulin syringe to deliver the reagents into the subarachnoid space between the L5 and L6 spinal levels. The instant tail-flick reaction induced by the needle entry was applied to valid a proper depth of the needle. For both of the two administration types, vehicle was applied alone to the control groups compared to the corresponding drug groups.

Adeno-associated viruses (AAV2/9-Iba1-zsgreen-sh*Tlr2* and AAV2/9-Iba1-zsgreen-NC) were designed and manufactured by HanBio (Shanghai, China). AAV injection was performed 4 weeks prior to behavioral tests. In brief, mice were deeply anesthetized under isoflurane (RWD Life Science, Guangdong, China) and a 30-G syringe was used to conduct intradermal/intrathecal injection to deliver AAV viruses ($1x10^{12}$ vg/mL, 10 μL). Once the injection finished, the syringe was maintained for 5 s and then removed.

Behavioral tests

Pain behavioral test

Mice were fully acclimated by being placed in the test chamber on the metal mesh 30 min before each behavioral assay. Mechanical allodynia was assessed by applying a series of von Frey filaments (0.16, 0.40, 0.60, and 1.00 g) to the plantar surface at a vertical angle for 3 s. Each mouse was tested 10 times and the percentage of paw withdrawal response was calculated. For the Hargreaves test, the radiant heat source of a thermal stimulator (BME-410C Plantar Test Apparatus) was focused on the hind paw for 3 times and the average withdrawal latency was calculated. The timeline of drug delivery and behavior test for each pharmacological experiment was showed by diagram in relative figures.

Itch behavioral test

To test the spontaneous itch and mechanical itch, the fur on the neck nape was carefully shaved without any skin lesions and mice were fully acclimated for 3 consecutive days by being placed in the plastic chamber 30 min per day. For the spontaneous itch, mice were immediately put into the chambers and recorded with a high-resolution digital camera (SONY HANDYCAM HDR-PJ580E, Japan) for 30 min. Scratching the nape skin with hind paws was defined as a single scratching bout. For the mechanical allokinesis, von Frey filaments ranging from 0.008 to 1.0 g were used to deliver mechanical stimuli. The filaments were applied to the nape skin for up to 1 s unless the scratching response. Each mouse was tested 5 times for every filament with a 10 s interval between adjacent two weights. The percentage of scratching responses was calculated.

Primary microglia transfection and drug administration

To test the effects of S2E, primary microglia was cultured with medium containing S2E (1.0 μg/mL) or Vehicle (PBS) for 12 h. To identify TLR2 function, siTLR2 or scRNA was transfected for 24 h before S2E addition. To pharmacologically block TLR2, primary microglia was treated by S2E together with C29 or its Vehicle (PBS containing 10% DMSO) for 12h before samples collection.

Immunofluorescence staining

Immunohistochemistry for cryosections

After 12 hours of S2E injection, mice were deep anesthetized with pentobarbital sodium and perfused with sterile PBS, followed by pre-cooled 4% paraformaldehyde (PFA, Servicebio, Wuhan, China). The lumbar segments (L3-L5) of the spinal cord, DRG, and hind paw skin were removed rapidly. After post-fixed in 4% PFA and dehydrated overnight in 30% sucrose, the tissues were embedded in OCT (Tissue-Tek, Japan) and cut into 15 μm sections. For the human samples, tissues collected from donors were fixed in 4% PFA. Sections were then permeabilized with 0.3% Triton X-100, blocked for 1 h at room temperature with 10% donkey serum, and incubated overnight at 4°C with primary antibodies. After PBS washing, sections were incubated with corresponding secondary antibodies for 1 h at room temperature. The slides were then mounted by mounting medium (ZSGB-Bio, Beijing, China) and scanned by a laser confocal microscopic imaging system (FV1000 and Olympus FluoView software; Olympus, Japan). At least 3 sections from each donor's sample or 10 sections from 3 randomly selected mice from each group were examined. The fluorescence intensity was measured with ImageJ.

The used primary antibodies included: rabbit anti-TLR2, 1:200, Abcam (ab209216); mouse Anti-His-tag, 1:200, MBL (D291-3); goat anti-IBA1, 1:400, Abcam (ab5076); Chicken anti-GFAP, 1:400, Abcam (ab4674); mouse anti-NeuN, 1:1000, Abcam (ab104224); mouse anti-c-Fos, 1:1000, Abcam (ab208942); rabbit anti-p-ERK, 1:400, CST (4370); rabbit anti-S2E, 1:500, Proteintech (28904); rabbit anti-S2S, 1:500, GeneTex (GTX635654); rabbit anti-S2M, 1:500, GeneTex (GTX636245); rabbit mAb isotype IgG, 1:500, CST(3900).

Immunohistochemistry for primary microglia

After pharmacological treatment, microglia were post-fixed in cold 4% PFA for 10 min. After permeabilized with 0.2% Triton X-100 for 15 min, the coverslips were incubated with 3% bull serum albumin (BSA, Solarbio, Beijing, China) for 20 min. Then the sections were incubated with primary antibodies at 4°C overnight. After washed by PBS buffer, these glass coverslips were incubated with corresponding secondary antibodies for 1 h and mounted with fluorescent mounting medium. Images were acquired and analyzed with laser confocal microscopic imaging system (TCS-SP8 STED 3X, Leica, Germany).

The used primary antibodies included: rabbit anti-p-NF-κB (Ser536), 1:400, CST (3033); rabbit anti-TLR2, 1:200, Abcam (ab209216); mouse anti-His-tag, 1:200, MBL (D291-3); goat anti-IBA1, 1:400, Abcam (ab5076).

The used secondary antibodies included: donkey anti-mouse Alexa 405, 1:400, Abcam (ab175658); donkey anti-rabbit Alexa 488, 1:400, Abcam (ab150073); donkey anti-rabbit Alexa 594, 1:400, Invitrogen (A-21207); donkey anti-mouse Alexa 594, 1:400, Abcam (ab150108); donkey anti-goat Alexa 594, 1:400, Abcam (ab150132).

RNA extraction and quantitative real-time PCR (qPCR)

Total RNAs of skin, spinal dorsal horn (SDH) and cultured microglia were extracted using TRIzol reagent (Invitrogen, USA), then reversely transcribed by RT Master Mix (Takara, Japan) according to the manufacturer's instructions. qPCR amplifications were conducted by CFX96™ Real-Time PCR Detection System (Bio-Rad, Hercules, California, USA) with MagicSYBR Mixture (Cwbio, Jiangsu, China). The housekeeping gene β-Actin was used for normalization. The primers were listed in Table S2.

Western blotting

12 h after S2E injection, mice were deep anesthetized with pentobarbital sodium (50 mg/kg i.p.). The spinal cord and skin were harvested rapidly and homogenized in T-PER tissue protein extraction reagent (Thermo Fisher Scientific, USA) with a protein phosphatase inhibitor and protease inhibitor cocktail. After denatured on heating, proteins were separated by 10% SDS-PAGE electrophoresis and transferred to polyvinylidene fluoride membranes. The membranes were blocked with BSA (Solarbio, Beijing, China) for 1 h at room temperature, and primary antibody (rabbit anti-NF-κB, 1:1000, CST (8242); rabbit anti-p-NF-κB (Ser536), 1:1000, CST (3033); rabbit anti-TLR2, 1:1000, Abcam (ab209216); mouse anti-β-Actin, 1:2000, CST (3700)) incubation was performed at 4°C overnight. The membranes were washed three times and incubated with the corresponding secondary antibody (HRP-conjugated goat anti-mouse, 1:3000, CST (7076); HRP-conjugated goat anti-rabbit, 1:3000, CST (7074)) for 1 h at room temperature. The bands were visualized with western blotting system (Cytiva, USA) after detected by eECL western blotting kit (Tanon, China).

QUANTIFICATION AND STATISTICAL ANALYSIS

Data were presented as means with standard errors (mean ± SEM). Statistical analyses were performed using the SPSS software (version 17.0). A Student's t test was used to evaluate the statistical significance of a difference between two groups. Comparisons for a group of multiple timepoints were carried out using a One-way ANOVA with Dunnett's multiple comparisons test. Comparisons for multiple groups with the control group were carried out using a Two-way ANOVA with Dunnett's post hoc test. Comparisons for multiple timepoints were carried out using a two-way ANOVA with Sidak's post hoc test. $p < 0.05$ was considered as statistical significance in all analyses. Significance levels (p values) are indicated in legends of each figure, showing *, $p<0.05$; **, $p<0.01$; ***, $p<0.001$; ****, $p<0.0001$; n.s., non-significant. All results of *in vitro* experiments were collected from at least 3 independent biological replicates.